(This is a sample cover image for this issue. The actual cover is not yet available at this time.)

Remote Sensing of Environment 132 (2013) 238–253

Contents lists available at SciVerse ScienceDirect

Remote Sensing of Environment

journal homepage: www.elsevier.com/locate/rse

Estimating variability in the quantum yield of Sun-induced chlorophyll fluorescence: A global analysis of oceanic waters

Yannick Huot [a,*], Bryan A. Franz [b], Maxime Fradette [c]

[a] Centre d'applications et de recherches en télédétection, Département de géomatique appliquée, Université de Sherbrooke, Sherbrooke, Québec, Canada J1K 2R1
[b] NASA Goddard Space Flight Center, Greenbelt, MD 20771, USA
[c] Département de physique, Université de Sherbrooke, Sherbrooke, Québec, Canada J1K 2R1

ARTICLE INFO

Article history:
Received 28 June 2012
Received in revised form 4 January 2013
Accepted 5 January 2013
Available online xxxx

Keywords:
Ocean color
Sun-induced fluorescence
Algorithm
Quantum yield

ABSTRACT

While empirical and semi-analytical algorithms that retrieve phytoplankton biomass from satellite ocean color have matured over the last few decades, the use of Sun-induced chlorophyll fluorescence data measured by spaceborne sensors remains in its infancy. Sun-induced fluorescence has the potential to provide a synoptic global view of aspects of phytoplankton biology that go beyond biomass by observing the quantum yield of fluorescence. While several algorithms have been developed to retrieve the quantum yield, they are prone to biases from different sources. In this study, we assessed the accuracy of several ocean color algorithms to estimate phytoplankton chlorophyll or absorption when they are used together with Sun-induced fluorescence algorithms. Our analysis led us to develop a new type of algorithm for retrieving variability in the quantum yield of fluorescence. Based on a three dimensional lookup table, this algorithm avoided many of the biases present in older algorithms and provided distributions of the quantum yield that showed significant differences compared to previous methods. This algorithmic approach also has the advantage of being robust with respect to sensor characteristics and to the set of underlying proxies that are used, namely phytoplankton biomass, the absorption by chromophoric dissolved organic matter, and the incident irradiance. As such, it would be suitable for merging data from multiple satellite ocean color sensors.

1. Introduction

As the biomass of phytoplankton in the surface water of the ocean increases, the color of the water shifts from violet-blue to green-olive. This shift is caused by the strong absorption of blue wavelengths by phytoplanktonic cells as well as their weaker absorption of green wavelengths (Morel, 1988; Yentsch, 1960), thereby reducing the amount of blue light backscattered out of the ocean to a greater extent than the green light. These shifts in the hues of water are quantifiable by in situ or remote measurements of the spectra of light leaving the ocean surface and can be used in algorithms to infer the phytoplankton biomass (Clarke et al., 1970). Such algorithms were first developed empirically (see O'Reilly et al., 1998 and references therein) by functionally relating the ratio of blue-to-green radiance (blue light near 440 or 490 nm; green light near 550 nm) leaving the ocean surface to the phytoplankton chlorophyll *a* concentration ([*chl*], mg chl m^3) measured in situ.

Phytoplankton is not the only component in water that influences the water color or the ratio of blue-to-green radiance leaving the water surface. Another group of constituents, generally referred to as chromophoric dissolved organic matter (CDOM), causes a similar effect because its spectral absorption monotonously increases towards shorter visible wavelengths (with high concentrations of CDOM turning the color of the water to brown). Empirical algorithms have gradually improved over the years to avoid biased estimates of phytoplankton biomass that are caused by either CDOM or colored detrital matter (CDM, which includes both CDOM and non-algal particulates). In recent versions, this is achieved by shifting the blue bands used in the ratio of radiance toward longer wavelengths as the color of the water becomes greener (i.e. the ratio of blue-to-green radiance decreases, c.f., 1998).

In the early to mid-1990s, a new group of ocean color algorithms was developed (e.g. Carder et al., 1991; Garver and Siegel, 1997; Roesler and Perry, 1995). These algorithms allow the use of the additional waveband on SeaWiFS (Sea-viewing Wide Field-of-view Sensor) and subsequent satellite sensors that is located near 412 nm (violet) to separate the absorption by phytoplankton from the absorption by CDM. These so called "semi-analytical" algorithms are based on established relationships (e.g. Gordon et al., 1988; Morel and Prieur, 1977) between the reflectance of water (or similar quantities) and the total absorption (a, m^{-1}) and backscattering (b_b, m^{-1}) coefficients of water, particles and dissolved matter within the water. They use the specific spectral characteristics (explicitly or not) of these constituents to retrieve the respective absorption and backscattering from the measured reflectance or remotely sensed reflectance. The estimates of phytoplankton biomass from these algorithms, whether in terms of phytoplankton

* Corresponding author. Tel.: +1 819 821 8000x65542; fax: +1 819 821 7944.
E-mail addresses: yannick.huot@usherbrooke.ca (Y. Huot), bryan.a.franz@nasa.gov (B.A. Franz), Maxime.Fradette@usherbrooke.ca (M. Fradette).

0034-4257/$ – see front matter © 2013 Elsevier Inc. All rights reserved.
http://dx.doi.org/10.1016/j.rse.2013.01.003

absorption coefficients (a_φ, m^{-1}) or chlorophyll *a* concentration should not, in principle, be influenced by the presence of CDM in the water. For remotely sensed data, this logical conclusion based on basic principles is hard to validate in practice due to the sparsity of validation datasets and measurement errors in these data. For example, despite having significant skill in estimating the absorption by CDOM (IOCCG, 2006; Siegel et al., 2005), estimates of phytoplankton biomass using semi-analytical algorithms do not typically show improved statistics when compared with empirical algorithms on validation datasets (e.g. Siegel et al., 2005). Three of these algorithms known as the Garver–Siegel–Maritorena model (GSM, Maritorena et al., 2002), the quasi-analytical algorithm (QAA, Lee et al., 2002), and the generalized IOP model are implemented as standard algorithms and their data products are distributed by the NASA Ocean Biology Processing Group. The latter, however, remains an experimental product at this stage and will not be examined in this study.

Outputs from empirical chlorophyll algorithms can be corrected for biases that arise due to the varying absorption by CDM at a given ratio of blue-to-green radiance (i.e. departures from the mean trend between the phytoplankton biomass and the absorption by CDM, Brown et al., 2008; Lee and Hu, 2006; Morel and Gentili, 2009). Since phytoplankton absorption increases between 400 and 443 nm whereas that of CDM decreases within this range, additional information available at the shorter wavebands (usually between 400 and 412 nm) can be used to distinguish between these two components (e.g. Morel and Gentili, 2009; Morel and Gordon, 1980). The essence of these approaches to correct empirical algorithms is to use the departures of measured reflectance spectra from a statistical "mean spectrum" for the same blue-to-green ratio. Though original ideas to correct empirical algorithms in this way predate the launch of the first ocean color sensor (reported later in Morel, 1980; Morel and Gordon, 1980), two such methods have been introduced recently (Brown et al., 2008; Morel and Gentili, 2009). The Φ index proposed by Morel and Gentili (2009 referred to as MG09 herein) is a correction for the effects of CDOM on chlorophyll estimates, when the chlorophyll estimates are obtained by a globally tuned empirical algorithm; it is currently implemented and distributed by NASA. The procedure proposed by Brown et al. (2008) requires further validation before implementation.

The launch of MODIS and MERIS sensors with new spectral bands in the red wavelengths allowed the observation of Sun-induced chlorophyll fluorescence (Babin et al., 1996; Gower and Borstad, 2004; Letelier and Abbott, 1996). Algorithms have been proposed (e.g. Abbott and Letelier, 1999; Babin et al., 1996) and applied (e.g. Behrenfeld et al., 2009; Gower et al., 2004; Huot et al., 2005; Morrison and Goodwin, 2010) to interpret this measurement in terms of phytoplankton biomass or the apparent quantum yield of fluorescence (φ_f^{app}, photons emitted [photons absorbed]$^{-1}$; the fraction of photons absorbed by phytoplankton reemitted as fluorescence). Mostly applicable to oceanic waters far from coastal influences, these algorithms are generally based on an analytical function (but see Gower et al., 2004) describing the radiance leaving the surface originating from fluorescence and a series of empirical relationships or semi-empirical relationships to constrain this function.

On the one hand, to use these algorithms the quantum yield of fluorescence must be known or estimated in order to retrieve the phytoplankton biomass. In coastal waters, it is difficult to estimate the chlorophyll concentration by standard ocean color algorithms because of the presence of significant concentrations of CDOM and non-algal particulate matter. In some of these waters, Sun-induced fluorescence could be used to estimate the phytoplankton biomass (e.g. Ahn and Shanmugam, 2007; Huot et al., 2007; Sathyendranath et al., 2004) by setting the quantum yield to some known value. In waters with high concentrations of CDOM or non-algal particulate matter concentration further difficulties arise in the estimation of the fluorescence radiance, which complicates the use of Sun-induced fluorescence (e.g. Gilerson et al., 2007; Ioannou et al., 2009; McKee et al., 2007).

On the other hand, the estimate of φ_f^{app} requires precise knowledge of a_φ. More accurate estimates of a_φ can be obtained using empirical or semi-analytical ocean color algorithms in ocean waters far from coastal influences; these oceanic waters are the sole focus of this article. The quantum yield can be retrieved in these waters, and it can potentially provide information about the physiology or the presence of groups of phytoplankton (the main source of variability in the quantum yield remains unknown and may vary regionally Behrenfeld et al., 2009; Letelier et al., 1997; Morrison, 2003; Schallenberg et al., 2008). Accurate estimates of φ_f^{app} and a_φ also require accounting in the algorithm for the reabsorption of fluorescence within the cell as well as the attenuation of incident spectral irradiance and the upwelling fluorescence radiance (see below).

In this paper, we focus on two variables: the concentration of chlorophyll *a* (or phytoplankton absorption) and the absorption coefficient of CDM (a_{CDOM}, m^{-1}), which can either bias or be retrieved by empirical and semi-analytical ocean color algorithms and Sun-induced fluorescence algorithms. With the ultimate goal of improving Sun-induced fluorescence algorithms to retrieve the quantum yield, we addressed the following question: What can be learned from Sun-induced fluorescence about chlorophyll algorithms and vice versa? In essence, the approach used to address this question relied on the theory underlying Sun-induced fluorescence to provide an independent means of statistically evaluating trends and dispersion observed in semi-analytical and empirical algorithms. This allowed us to assess the different remote sensing estimates of phytoplankton absorption required by fluorescence algorithms to estimate φ_f^{app}. We began by examining two standard empirical ocean color algorithms (OC2M and OC3M). These algorithms use respectively two (489 and 547 nm) and three bands (443, 489 and 547 nm). In the case of the latter, the maximum band ratio (MBR, unitless) is used as the independent variable and is defined as the ratio of the highest value of remote sensing reflectance (R_{rs}, sr^{-1}) at either 443 nm or 489 nm to R_{rs} at 547 nm. We then examined the effect of the correction proposed by Morel and Gentili (2009) on these algorithms (referred to as the Φ-corrected OC2M and Φ-corrected OC3M). Since our analysis was improved by accurately correcting the Sun-induced fluorescence measurement for the incident irradiance, we also examined the influence of incident irradiance on Sun-induced fluorescence. These results showed that Sun-induced fluorescence could be used as a tool to improve semi-analytical algorithms. Finally, we proposed a new algorithmic approach to measure variability in the quantum yield of fluorescence using satellite measurements. This algorithm should, in our opinion, supersede algorithms such as Huot et al. (2005) and others using a similar approach for the analysis of variability in the quantum yield of fluorescence from satellite remote sensing for most applications.

2. Background

2.1. Sun-induced emission at the sea surface

Following a few assumptions (e.g. Huot and Babin, 2010; Kishino et al., 1984; Maritorena et al., 2000; Zhou et al., 2008), the fluorescence radiance (L_f) just below the sea surface at nadir can be expressed as

$$L_f = \frac{1}{4\pi} a_\varphi Q_a^* \overset{o}{E}_{PAR}(0^-) \frac{1}{K_{abs}^{\tau_f} + a_f}; \quad (1)$$

where Q_a^* (unitless) is the fraction of fluorescence leaving the cell without being reabsorbed, $\overset{o}{E}_{PAR}(0^-)$ is the scalar photosynthetically available irradiance (PAR, irradiance integrated spectrally between 400 and 700 nm, $\mu mol\ m^{-2}\ s^{-1}$) just below the surface, $K_{abs}^{\tau_f}$ (m^{-1}) is the attenuation of scalar irradiance within the uppermost part of the water column where fluorescence radiance originates, and a_f (m^{-1}) is

the absorption coefficient for upwelling radiance within the fluorescence band.

In case 1 water (defined in Morel and Prieur, 1977) far from terrestrial influences, relationships have been developed between the phytoplankton abundance estimated in terms of chlorophyll and the following variables (Huot et al., 2005 and references therein): a_φ, Q_a^*, and $K_{abs}^{\tau_f}$. These relationships represent mean trends, but a significant amount of variability around these trends is observed due to the variable nature of the species composition and physiology of phytoplankton at a given chlorophyll concentration. In addition, $K_{abs}^{\tau_f}$ is essentially a diffuse attenuation coefficient weighted by phytoplankton absorption, and variability can arise from other absorbing components, in particular CDM. As with any diffuse attenuation coefficient, $K_{abs}^{\tau_f}$ is directly proportional to the total absorption coefficient (e.g. Gordon, 1989). The influence of the colored components is much less important in the case of a_f because of the overwhelming influence of water absorption in the fluorescence band for most oceanic waters. It is also important to note that, despite a significant amount of variability in case 1 waters, general trends exist between phytoplankton biomass and absorption by CDOM (Morel, 2009; Morel and Gentili, 2009) and CDM (Siegel et al., 2005). Noting that CDOM absorption is the dominant fraction of CDM absorption (Siegel et al., 2002) in case 1 waters, we will mostly ignore the distinction between the two in what follows. However, we will try to acknowledge throughout this paper where different algorithms were meant to estimate CDOM (MG09) or CDM (GSM and QAA, see below for definitions of these algorithms) and we will thus use both abbreviations. Because we focus on case 1 waters with limited terrestrial influences, we will ignore the potential effect of high scattering by non-algal particulates which can influence the retrieval of fluorescence radiance (Gilerson et al., 2007; McKee et al., 2007).

2.2. Influences on and potential biases in estimates of the quantum yield

2.2.1. Phytoplankton biomass

Using Eq. (1) and solving for φ_f^{app} requires estimating all of the other variables. In the case of phytoplankton biomass, this is done either in terms of [*chl*] or a_φ by direct application of an algorithm on measurements of upwelling radiance. When [*chl*] is retrieved, the relationship $a_\varphi = [chl]a_\varphi^*$ is used, where a_φ^* (m^2 mg chl^{-1}) is the chlorophyll specific absorption of phytoplankton. For the other variables (including a_φ^*), the empirical relationships mentioned above are used. In the ocean, the variable that varies the most – by 3 orders of magnitude – is the phytoplankton biomass. Errors in the estimate of the chlorophyll concentration or the phytoplankton absorption propagate directly (see Eq. (1)) to estimates of φ_f^{app}. The quantum yield of fluorescence at the surface appears to vary at most by about a factor of 10, and possibly less, under remote sensing conditions (Huot et al., 2005; Maritorena et al., 2000; Morrison, 2003; Morrison and Goodwin, 2010; Ostrowska et al., 1997; Schallenberg et al., 2008). Any biases in the estimates of [*chl*] could thus lead to important biases in the retrieval of φ_f^{app}.

2.2.2. Influence of CDM in case 1 waters

The direct influence of CDM on chlorophyll fluorescence radiance leaving the sea surface originates from its effect on $K_{abs}^{\tau_f}$. An indirect influence on the retrieval of φ_f^{app} using ocean color algorithms can also originate from biased estimates of the phytoplankton biomass. With empirical algorithms, the presence of a higher than normal CDM concentration, for a given blue-to-green ratio, will lead to an overestimate of [*chl*] or a_φ. When applying Eq. (1), this will lead to an underestimate of φ_f^{app}. Similarly, with these algorithms an underestimate of the phytoplankton absorption due to a lower than average CDM concentration will lead to an overestimate of φ_f^{app}.

3. Data and statistics

3.1. Satellite datasets

We downloaded MODIS Aqua mapped daily Level-3 data products (reprocessing 2009.1) at 4 km spatial resolution from the NASA ocean color website (http://oceancolor.gsfc.nasa.gov) for each day of 2007. This dataset included the following data products: the chlorophyll concentration (mg chl m^{-3}) from both the OC3M-547 algorithm (herein referred to as OC3M, http://oceancolor.gsfc.nasa.gov/REPROCESSING/R2009/ocv6/) and the GSM algorithm (GSM, Maritorena et al., 2002); the phytoplankton absorption coefficient at 443 nm (m^{-1}) from the QAA algorithm (QAA, Lee et al., 2002); the Φ index (dimensionless; the chromophoric dissolved organic matter index product, Morel and Gentili, 2009); the absorption by CDM from the QAA and GSM algorithms ($a_{CDOM}(443)$, to simplify the notation we use the subscript "CDOM" for both the CDM and CDOM absorption estimates); the calculated planar photosynthetically available radiation ($E_{dPAR}(0^+)$, converted to μmol m^{-2} s^{-1}) just above the water surface at the time of the image (distributed by NASA as the iPAR product); the fluorescence line height extracted from the normalized water leaving radiance (the nFLH product, as per Behrenfeld et al., 2009); and the remote sensing reflectances ($R_{rs}(\lambda)$, sr^{-1}) at 412, 443, 488, 547 and 667 nm. From these reflectances, the chlorophyll estimates from the OC2M algorithm (herein referred to as OC2M) were computed following the equations provided at (http://oceancolor.gsfc.nasa.gov/REPROCESSING/R2009/ocv6/).

The data used herein are slightly different from previous studies. Before our study, in the standard NASA production of Level-3 *nFLH* products, all negative *nFLH* retrievals were set to zero prior to computing the Level-3 mean. Since these negative retrievals were found to represent an increasing fraction of the pixels with decreasing chlorophyll and did not appear to depart from the normal distribution of the data, we believe these values are valid and probably result from noise in the sensor. We thus reprocessd all Level-3 *nFLH* scenes to include the negative values in the averages except above 1 mg chl m^{-3} where they are clearly outliers. The effect of this change is seen only below about 0.1 mg chl m^{-3}, where it, however, significantly changes the relationship between *nFLH* and chlorophyll concentration. It is also important to note that the current iPAR product distributed by NASA is not the product described in the original iPAR algorithm theoretical basis document (Carder et al., 2003). Rather, it is derived by integration of the product of extraterrestrial solar irradiance (Thuillier et al., 2003) atmospheric transmittance(Ahmad et al., 2007; Gordon and Wang, 1994), and the cosine of the solar zenith angle. The integration is performed over the spectral range from 400 to 700 nm at 1 nm intervals. The atmospheric transmittance is determined at each sensor band during the atmospheric correction process, and then interpolated to 1 nm increments for the integration. A major difference (discussed later) compared with the previous iPAR algorithm is that $E_{dPAR}(0^+)$ is computed above the surface.

A matrix of 56,963,511 lines (pixels) and 13 columns (data products) was obtained by randomly sampling each of the 365 daily Level-3 sets of global images. The random selection of pixels was weighted in the following manner to avoid observational biases (e.g. clouds, masked data) and to obtain a dataset that was as evenly spatially distributed as possible (high latitude seasonal biases were unavoidable). For all daily images during 2007, a probability map of not observing a pixel was calculated as N_{notobs}/N_{tot}, where N_{notobs} is the number of masked pixels observed during the year and $N_{tot} = 365$ is the total number of times this pixel was present in the dataset. When loading each image, a matrix of random numbers (uniformly distributed between 0 and 1) was created that was the same size as the image. A pixel was selected if the random number was smaller than the value on the probability map for the same pixel.

We applied the following cut-off to the dataset to exclude outliers and aberrant data: all physical limits (except for *nFLH*) had to have

values greater than 0 and the Φ-index had to be smaller than 7 (thereby excluding waters with excessively strong coastal influences). Furthermore, we discarded pixels that differed by more than 0.3% between the chlorophyll concentration computed by applying the OC3M algorithm directly to the downloaded Level-3 remote sensing reflectances and the chlorophyll concentration from the same products distributed by NASA but derived from the Level-2 products and then averaged to obtain Level-3. These quality control measures left a total of 47,030,638 pixels. All analyses, except when we applied our algorithm to new images, were carried out on data from this matrix.

3.2. SeaBASS dataset

From the SeaBASS (SeaWiFS Bio-optical Archive and Storage System) archive (http://seabass.gsfc.nasa.gov/), we downloaded the chlorophyll concentration measured in situ and the matchup *nFLH* product (a total of 510 points) from the MODIS Aqua sensor.

3.3. Statistics

To provide an estimate of the variability present in the relationship between different estimates of chlorophyll and *nFLH* we computed the median trend line and compute the relative median absolute deviation (RMAD Rousseeuw and Croux, 1993) from this trend line as:

$$RMAD = 100{*}med|\{nFLH_i - med_{nFLH}([chl_i])\}/med_{nFLH}([chl_i])| \quad (2)$$

where "med" represents the "median value of" and $med_{nFLH}([chl_i])$ is the median trendline evaluated at the *i*th *nFLH* point $nFLH_i$. RMAD can be interpreted as the relative difference from the trend line within which 50% of the points fall. It is akin to a mean absolute percent error but more robust to outliers.

4. Results

4.1. The OC2M algorithm as a benchmark

The relationship between *nFLH* and the chlorophyll estimated from the OC2M algorithm (Fig. 1) was used as a benchmark against which we evaluated other algorithms to estimate the chlorophyll concentration. For several of the following plots, median values (black dots) and mean values (black X's) were computed for 70 equally spaced (in log space) bins throughout the range of the measured chlorophyll values. This approach using the median values was selected because it provided a better representation of the trend compared to a standard nonlinear fitting approach due to the non-normal distribution of the residuals. Robust fitting procedures provided very similar results depending on the tuning parameters that were used. However, the median approach provided a more objective and general approach as we progressed with the analysis. Data from the SeaBASS matchup dataset (scattered gray points) as well as a scaled theoretical line (magenta) from the model of Huot et al. (2005) are superimposed on Fig. 1.

Fig. 1 shows that the theoretical model is very similar to the mean and median values between $0.1<[chl]<3$ mg chl m^{-3}. Above and, below this range the trends depart significantly from the theoretical model. Near 0.1 mg chl m^{-3}, the data show a rapid decrease with chlorophyll and then a much lower slope than is expected theoretically. This is significant because, based on the dataset used here, around 45% of the ocean surface has a chlorophyll concentration below 0.1 mg chl m^{-3} (see also Antoine et al., 2005). Above 3 mg chl m^{-3}, the departure from the theoretical model is of much less concern because the areal fraction of the ocean with a surface chlorophyll concentration above this value is approximately 6%. However, the departure is much greater in this region. The magenta line of the theoretical model passes approximately through the center of the points from the SeaBASS matchup dataset despite significant variability, especially at low chlorophyll concentrations. For [*chl*] above 3 mg chl m^{-3}, the departure of the median (and mean) trend from the theoretical line can be attributed almost certainly to biases in the remote estimates of chlorophyll because the chlorophyll values measured in situ are not biased by remote sensing artifacts; this follows logically since the median line also departs from the match-up dataset while the theoretical line goes through the center of the points. The large variability in the match-up dataset at low chlorophyll concentrations does not allow any such interpretation.

The lines formed by the median and mean points represent, in addition to the effect of biomass, the average change of several optical and

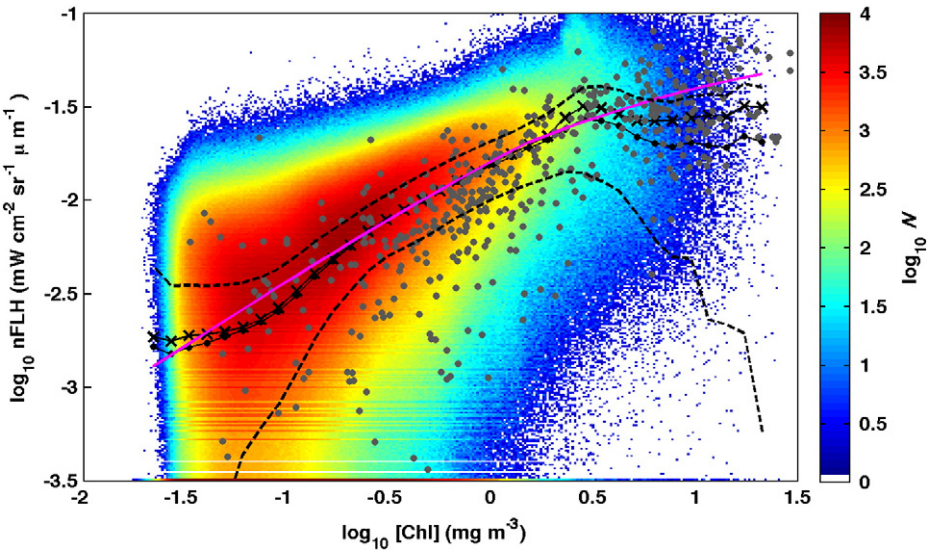

Fig. 1. Relationship between the *nFLH* data product measuring chlorophyll fluorescence at the sea surface and the chlorophyll concentration obtained from the OC2M ocean color algorithm. Black filled circles represent the median of the data falling within equally spaced bins of chlorophyll values extending from half the distance to and from the two adjoining points. The black X's represent the mean of the data for the same interval. The dashed lines represent the median ± the interquartile range. The magenta line is the scaled theoretical model of Huot et al. (2005) for the relationship between *nFLH* and [*chl*] scaled such that it matches the median value of *nFLH* at 0.5 mg chl m^{-3}. The gray points are from the SeaBASS validation dataset for the MODIS AQUA sensor (http://seabass.gsfc.nasa.gov/, accessed 28/10/2010). Colors represent the logarithm in base 10 of the number of points (*N*) within a bin. (For interpretation of the references to color in this figure legend, the reader is referred to the web version of this article.)

physiological parameters. It accounts (see Eq. (1)) for trophic changes in (Babin et al., 1996; Huot et al., 2005): φ_f^{app} (including the effect of photoprotective pigments), Q_a^*, a_φ^*, $K_{abs}^{\tau_f}$, a_f, as well as potential biases in the estimate of the baseline (Huot et al., 2005; Ioannou et al., 2009). Indeed, it could be seen as an "improved" representation of the "theoretical" trendline from Huot et al. (2005) that includes observational biases as well as trophic changes in φ_f^{app}. To obtain the quantum yield, most recent algorithms divide the fluorescence data by the value of some variant of this theoretical (unscaled) trendline. Therefore, any systematic departure from this trendline will translate into systematic changes in the quantum yield, which, in the case of chlorophyll-based algorithms would be dependent on the chlorophyll concentration. The variability in *nFLH* not accounted for by the trendline originates from: measurement errors in both chlorophyll and *nFLH* (including biases caused by CDM); departures of the optical characteristics of the water at a given band ratio (arising, for example, from the departure of CDM from the mean relationship); and variability in φ_f^{app}. Improving the retrieval of the latter requires reducing the errors in the estimates of the others. In that sense, in a global context, a trendline such as the mean or median in Fig. 1 provides an attractive alternative to the theoretical model as it can account for some of the biases present (e.g. non-zero values of *nFLH* at [*chl*] = 0). However, other biases such as those caused by CDOM must be removed from this trendline.

The most obvious source of variability in φ_f^{app} is the incident irradiance, which at high values (relative to the mean growth irradiance) leads to a decrease in the fluorescence quantum yield caused by non-photochemical quenching (e.g. Krause and Jahns, 2004). Such a decrease is clearly observed when the ratio of the data in Fig. 1 to the median line (i.e. ε_{chl} = *nFLH*/median trendline, unitless) is plotted against the photosynthetically active incident planar irradiance just above the sea surface $E_{dPAR}(0^+)$ (Fig. 2). The trend for most of the range of $E_{dPAR}(0^+)$ values decreases from a value of ε_{chl} of about 1.70 at 600 μmol m^{-2} s^{-1} to a value of 0.82 at 2000 μmol m^{-2} s^{-1}. Beyond 2000 μmol photons m^{-2} s^{-1}, there is a rapid and unexplained (it is not investigated in this study) rise in ε_{chl}. Superimposed on the median of this relationship (black points) is a power law best fit curve (gray) and the theoretical relationship (blue line) used by Behrenfeld et al. (2009); evidently, these curves are similar. It must, however, be kept in mind that while the trend observed in ε_{chl} with $E_{dPAR}(0^+)$ is consistent with non-photochemical quenching it is not the only possible source of this trend as other variables in Eq. (1) and remote sensing biases could covary with incident irradiance.

The general trend with $E_{dPAR}(0^+)$, however, when examined more closely, varies as a function of the trophic state of the ocean. This is highlighted in panels D and E of Fig. 2 where the same graph as for panel A is shown, but only for the data falling between 0.1 and 0.15 mg chl m^{-3} in panel D and 1.0 to 1.5 mg chl m^{-3} in panel E. The variation with $E_{dPAR}(0^+)$ is stronger at the lower chlorophyll concentrations. Median values of ε_{chl} (such as those presented in panels D and E) can be computed for small intervals of chlorophyll and $E_{dPAR}(0^+)$; applying this computation provided a more general representation of the variability in the median *nFLH* values as a function of $E_{dPAR}(0^+)$ (panel F). This figure highlights significant trends with incident irradiance in ε_{chl} which are at least partly originating from changes in φ_f^{app}. This is particularly obvious below ~0.1 mg chl m^{-3}, although interpretations at these [*chl*] must be made with extreme care (see Appendix 2). Above approximately 2 mg chl m^{-3}, no obvious trends with irradiance are apparent and the median values become more noisy (panel F).

The other source of variability that can be examined using this dataset originates from variability in CDM absorption at a given phytoplankton absorption. As mentioned previously, in case 1 waters, the consequence of such variability on the fluorescence estimates is twofold. Firstly, due to its influence on the ratios used in empirical algorithms, it biases the estimates of phytoplankton biomass that are used to normalize the fluorescence measurement to obtain φ_f^{app}. Secondly, at sufficiently high CDM concentrations, it affects $K_{abs}^{\tau_f}$ and thus decreases the fluorescence emission simply by a decrease of the irradiance present in the water. The second effect can be readily modeled for various CDOM absorptions by calculating the ratio (γ_{CDOM}, unitless)

$$\gamma_{CDOM} = \frac{\overline{K}_{abs}^{\tau_f} + \overline{a}_f / \cos\left(\theta'\right)}{{}^{\Delta CDOM}\overline{K}_{abs}^{\tau_f} + {}^{\Delta CDOM}\overline{a}_f / \cos\left(\theta'\right).} \quad (3)$$

where $\overline{K}_{abs}^{\tau_f}$ and $\overline{a}_f$ are values for mean CDOM concentrations at a given chlorophyll concentration in the ocean, and ${}^{\Delta CDOM}K_{abs}^{\tau_f}$ and ${}^{\Delta CDOM}a_f$ are the same variables but with more or less CDOM than the average. This ratio provides the relative increase or decrease in the expected fluorescence radiance due only to the addition or removal of CDOM from the mean CDOM concentration (in this case at a given chlorophyll concentration). Practical details of the approach used to model this ratio are given in Appendix 1. This simple model (magenta area) is compared (Fig. 3) with the ratio of the data shown in Fig. 2A by the surface in Fig. 2. F for different intervals of the chlorophyll concentration (see text within each panel). This ratio is referred to as $\varepsilon_{chl,ipar}$. The considerable amount of variability makes it difficult to see the match; however, the median line clearly illustrates that the trends caused by changes in CDOM absorption were much stronger in the observations (black line) than the theory (magenta area) would allow. By far, the most probable reason for such an observation is an underestimate of the chlorophyll concentration at lower values of CDOM absorption (than the mean trend with chlorophyll) and overestimates at higher CDOM absorptions values. In other words, unsurprisingly, the OC2M algorithm cannot correctly separate CDOM from chlorophyll and this is reflected in biases in the estimates of [*chl*]. Another indirect effect of CDOM that has not been mentioned is the potential change in φ_f^{app} arising from a reduced irradiance resulting from a change in the attenuation coefficient. In this case, we expect (i.e. as observed in Fig. 2) an increase in φ_f^{app} when the irradiance decreases (i.e. the attenuation coefficient increases). We assessed this effect using the result from Fig. 2 and Eq. (1) and found that the effect was small at most a 10% increase in fluorescence emission at very high CDOM, but generally much less (~1% at CDOM absorption values present in case 1 waters). We thus ignored this potential effect in the remainder of the paper but note that it was inherently accounted for in the new algorithm developed in Section 4.3.

4.2. Comparison with other algorithms

Other algorithms, whether empirical corrections to OC2M or semi-empirical algorithms, were evaluated by comparison with the results presented above. Five such algorithms are shown in Fig. 4. In panel A, the Φ-corrected OC2M chlorophyll estimates (using the Morel and Gentili, 2009, equation in the legend of their Fig. 9) show an improved match to the theoretical curve. There is also a reduced dispersion as reflected by the reduced RMAD compared to OC2M (column 2 of Table 1). It is important to recall (see Data and statistics) that the RMAD is calculated with respect to the median line and not the theoretical data. It thus provides a mesure of disperson around the median trend and not a measure of the match to the theoretical model. The OC3M algorithm (panel B) has a slightly greater departure similar to the OC2M algorithm at high chlorophyll values (both algorithms use the same reflectance ratio in this region), but it shows a similar relationship at low chlorophyll concentrations (continuously decreasing values that are more in accordance with theoretical expectations). Applying the Φ correction to the OC3M algorithm leads to an overall improvement of the fit to the theoretical line, except around 0.1 mg chl m^{-3}, and leads to the lowest RMAD (column 2 of Table 1) of all the empirical algorithms tested. In panel D, *nFLH* versus the chlorophyll estimates from the GSM algorithm closely follow the trend of the theoretical model at high chlorophyll but shows, like the Φ-corrected OC3M, an

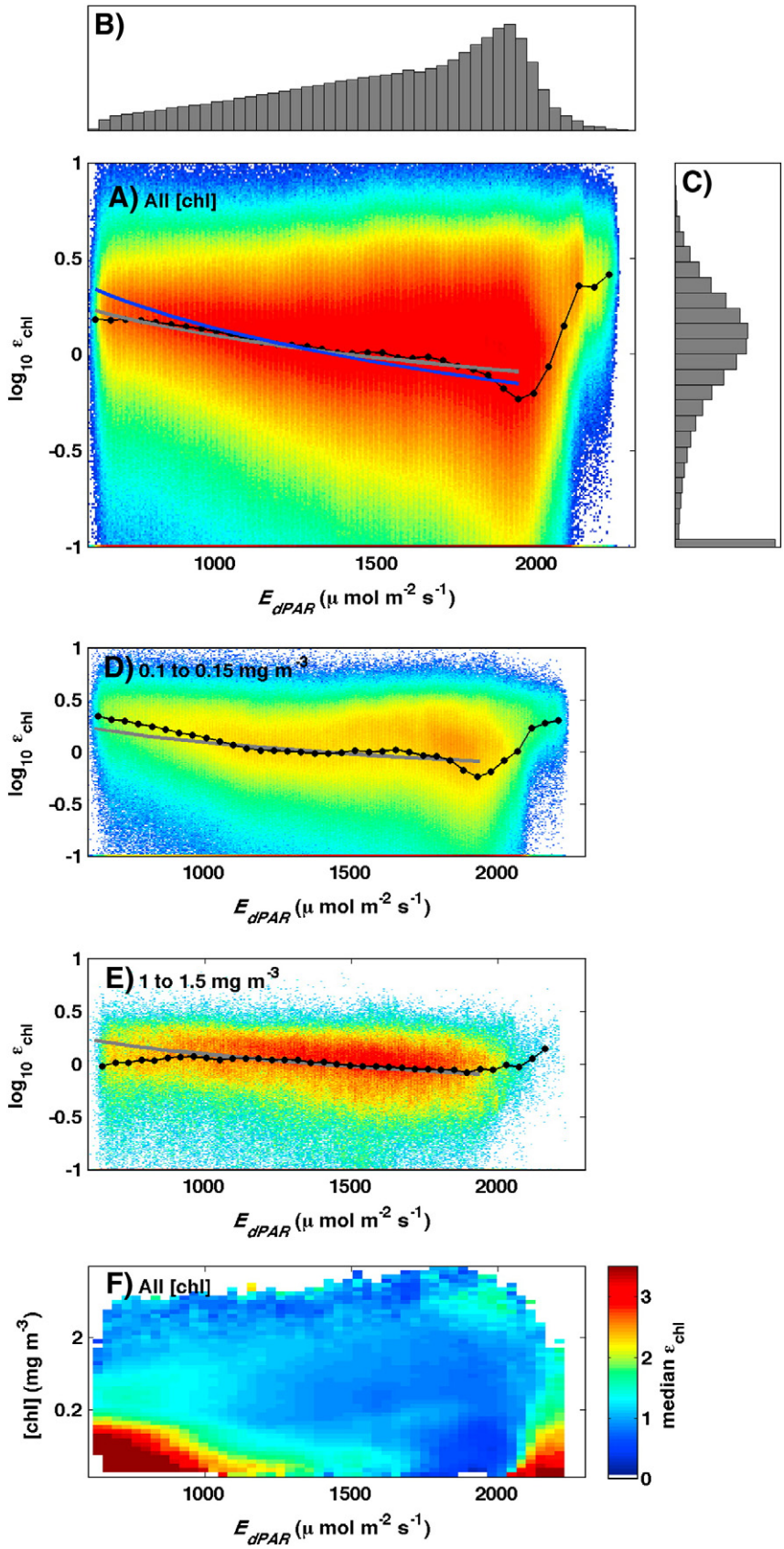

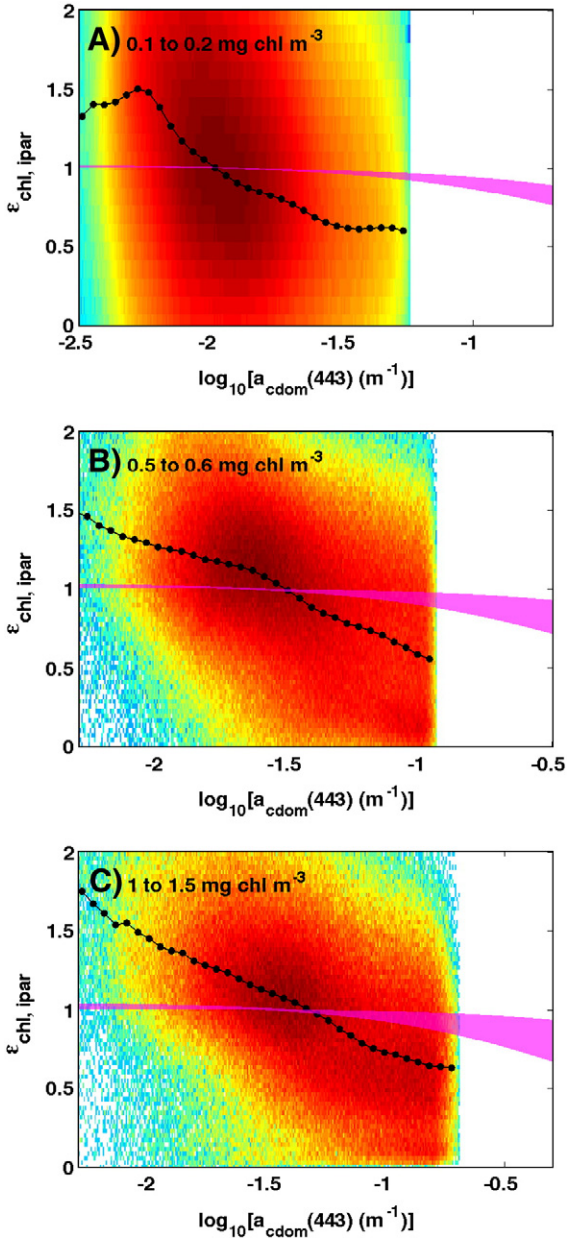

Fig. 3. Ratio calculated by dividing ε_{chl} by the median of ε_{chl} (obtained by interpolating the surface in Fig. 2F) plotted against the CDOM concentration (obtained by applying the algorithm in Morel and Gentili, 2009). Black line, density, and colors are the same as for Fig. 1. The magenta region represents the theoretical effect of CDOM on the measurement of fluorescence if the data were only affected by the effect of CDOM on the propagation of irradiance in the ocean (see Appendix 1 and Section 4.3 for details).

underestimate at low chlorophyll concentrations (see Discussion for a possible theoretical explanation). The GSM algorithm (see column 2 of Table 1), leads to the lowest RMAD of all the algorithms compared in this study. The estimates from the QAA algorithm (Fig. 4E) also improve the match to the theoretical model and reduced the RMAD compared to the OC2M algorithm, although the upper range does not seem to be as good as the GSM algorithm.

We do not show a systematic comparison of the trend with $E_{dPAR}(0^+)$ as all models showed similar results to the OC2M algorithm (see Fig. 2), albeit with a slightly lower standard deviation of the residuals for these algorithms (see column 3 of Table 1 for the statistics). The exponent of the power law's best fit line for each model was always higher (column 5 of Table 1) for the other algorithms compared with OC2M, bringing them closer, although always lower, to the relationship used by Behrenfeld et al. (2009). In the following analyses where we examined the effect of CDM, a model-specific correction for $E_{dPAR}(0^+)$ was applied to each model using a surface derived from an analysis equivalent to that carried out in Fig. 2E but for the ratio from their respective chlorophyll or phytoplankton absorption estimates.

Figs. 5 and 6 present a comparison of the trends of $\varepsilon_{chl,ipar}$ for four of the algorithms presented in Fig. 4 (Φ-corrected OC2M, Φ-corrected OC3M, GSM and QAA) with respect to the CDOM absorption. These figures can be compared to Fig. 3. Although not presented here, the results from the OC3M algorithm qualitatively resembled those from the OC2M algorithm. Applying the Φ correction to the OC2M and OC3M algorithms (Fig. 5) strongly reduced the deviations from the model observed in Fig. 3.

The same analysis for the GSM algorithm provided unexpected results. The adherence to the modeled trends was improved relative to Fig. 3 when the CDOM absorption was calculated using the MG09 method (not shown). However, when CDM was calculated using the GSM algorithm (left panels of Fig. 6), strong departures were observed from the theoretical line. The QAA algorithm was an intermediate case where improvement relative to the OC2M case was seen for both the MG09 CDOM algorithm (not shown) and the QAA estimates (right panels of Fig. 6). Explaining the results regarding the retrieval of $a_{CDOM}(443)$ with the semi-analytical algorithms was beyond the scope of our study. However, our analysis showed that Sun-induced fluorescence can be used as a general guide to improve ocean color algorithms to retrieve phytoplankton absorption or chlorophyll. Indeed the two analyses presented above allow comparing different versions of an algorithm or different algorithms on a large dataset. This can be done as in Fig. 1 by comparing the dispersion around the mean or median trendline of the data (as shown in Table 1) or by carrying out an analysis similar to that in Fig. 3 to examine the effect of biases caused by CDOM on the retrieval of chlorophyll. Finally, it should be noted that the significant variability captured by the CDM variable derived from the semi-analytical algorithms in the present study (even though it probably contains some biases) implies that it was retrieving an optical signal (likely linked to absorption) that causes important trends in *nFLH*.

4.3. A new algorithm for studying variability in the quantum yield of fluorescence

Given the results above, we developed a new approach based on the maximum band ratio that underlies the OC3M algorithm and a CDM correction (similar to that obtained by applying the Φ index). This approach appeared to provide one of the best foundations for developing a new algorithm. Although an approach based on the MBR had a slightly higher RMAD of the estimates (see column 4 of Table 1), after applying the chlorophyll and $E_{dPAR}(0^+)$ dependency of *nFLH*, the results were closer to those expected compared to semi-analytical models with respect to $a_{CDOM}(443)$.

Given the nonlinear and complex relationships between *nFLH*, chlorophyll, $E_{dPAR}(0^+)$, and $a_{CDOM}(443)$, our approach included a three dimensional lookup table (LUT) that "slices" the *nFLH* into portions

Fig. 2. A) Logarithm of the ratio (in normal space) of the *nFLH* data to the trendline for the median data in Fig. 1 plotted against the PAR irradiance just above the sea surface ($E_{dPAR}(0^+)$ from the iPAR data product). The blue line is the relationship used by Behrenfeld et al. (2009) and the gray line is the best fit for the median points (black points, $\varepsilon_{chl} = 80.6 E_{dPAR}(0^+)^{-0.61}$). B) Distribution of $E_{dPAR}(0^+)$. C) Distribution of ε_{chl}, where σ represents the standard deviation. D) Same as panel A but only for points between 0.1 and 0.15 mg chl m^{-3}. The gray line is reproduced from panel A. E) Same as panel D but for points between 0.5 and 0.6 mg chl m^{-3}. F) Surface of the median of ε_{chl} (colorbar scale) as it varies with $E_{dPAR}(0^+)$ and [*chl*]. This surface is used as a two dimensional LUT in the analysis of the effect of CDOM (see Fig. 3). We assigned a ε_{chl} value (color) only to bins that had at least 50 points. Negative data and values below −1 are all pooled together for graphing purposes on the first horizontal bin in panels A, C, D and E. (For interpretation of the references to color in this figure legend, the reader is referred to the web version of this article.)

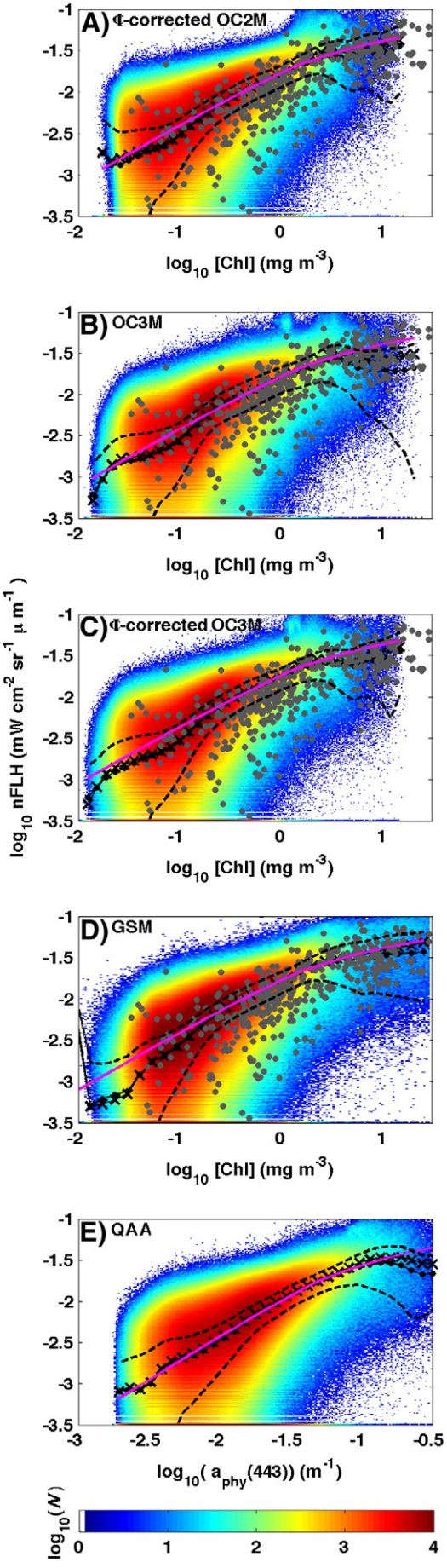

Table 1
Relative median absolute deviation (RMAD) between the different relationships representing the median trend in the *nFLH* data and the *nFLH* data (columns 2 to 4) as well as the average dependence of *nFLH* on irradiance (column 5).

Algorithms (chl; CDOM)[a]	[*chl*][b] chl > 0.1, all chl	$E_{dPAR}(0^+)$[c] chl > 0.1, all chl	LUT[d] chl > 0.1, all chl	$E_{dPAR}(0^+)$[e] "slope" chl > 0.1, all chl
OC2M; MG09	43.3, 53.6	40.7, 51.8	37.4, 49.1	−0.57, −0.64
Φ-corrected OC2M; MG09	42.1, 52.7	*38.4*, *50.4*	37.3, 49.2	−0.63, −0.68
OC3M; MG09	43.7, 53.8	40.8, 51.9	36.0, 47.9	−0.67, −0.72
OC3M; GSM	"	"	36.0, 47.9	"
OC3M; QAA	"	"	36.6, 48.5	"
Φ -corrected OC3M; MG09	*41.5*, *52.5*	37.3, 49.8	36.1, 48.2	−0.74, −0.77
Φ-corrected OC3M; GSM	"	"	36.4, 48.6	"
Φ-corrected OC3M; QAA	"	"	36.2, 48.4	"
GSM; MG09	**39.9, 50.9**	**36.4, 49.0**	34.9, 46.9	−0.72, −0.74
GSM; GSM	"	"	**34.7**, **46.6**	"
GSM; QAA	"	"	34.8, 46.8	"
QAA; MG09	41.9, 52.1	37.1, 49.6	36.0, 48.0	−0.79, −0.83
QAA; GSM	"	"	35.9, 48.0	"
QAA; QAA	"	"	36.0, 48.1	"
MBR; 412/443	43.7, 53.8	40.7, 51.8	*35.9*, *48.0*	−0.67, −0.72

[a] Algorithms used to compute the chlorophyll concentration and CDOM absorption at 443 nm.
[b] RMAD of the *nFLH* from the median trendline as a function of [*chl*]. The two numbers represent the RMAD value for [*chl*] greater than 0.1 and for all [*chl*] To have the same points for all algorithms, the Φ-corrected OC3M algorithm was used to identify the points.
[c] RMAD of the $\varepsilon_{chl,ipar}$ from the surface representing the $\varepsilon_{chl,ipar}$ as a function of [*chl*] and $E_{dPAR}(0^+)$. For the first row this is equivalent to estimating the RMAD between the point in Fig. 2A and the surface in Fig. 2F at their respective [*chl*] and $E_{dPAR}(0^+)$ values.
[d] RMAD of the *nFLH* from the look-up table estimate of $nFLH_{LUT}$. See point *b* above for details.
[e] Exponent of the power law dependence of *nFLH* on $E_{dPAR}(0^+)$ after removing the dependence on chlorophyll. For the first row, this is the power law exponent of the gray line in Fig. 2A.

that were greater and lower than a median ocean pixel for a given combination of [*chl*], $E_{dPAR}(0^+)$ and $a_{CDOM}(443)$. This approach, using three dimensions instead of one, was akin to that used by Brown et al. (2008) to study the sources of variability in ocean color. The axes chosen to represent chlorophyll and CDM were inspired by those proposed by Morel and Gentili (2009) for their Φ correction: one axis was MBR, the measure of phytoplankton absorption (replacing the ratio of $R_{rs}(489)$ to $R_{rs}(555)$ ratio in MG09); another axis was the ratio of $R_{rs}(412)$ to $R_{rs}(443)$ ($^{412}_{443}R_{rs}$), the measure of CDM; and the last axis was $E_{dPAR}(0^+)$, which is the output from the NASA iPAR algorithm. Using these axes, we obtained a lookup table of the median value of *nFLH* ($nFLH_{LUT}$, mW cm^{-2} sr^{-1} µm^{-1}) within each cube on a three dimensional grid (see Fig. 7). Using this LUT, for any pixel the value of $nFLH_{LUT}$ could be computed by interpolating the LUT and the *nFLH* value measured from that pixel was divided by $nFLH_{LUT}$. We thus obtained a new fluorescence number, χ_{fluo}, as:

$$\chi_{fluo} = nFLH/nFLH_{LUT} \tag{4}$$

We developed, in parallel, a series of LUT-based algorithms with three inputs ([*chl*] or a_φ, $a_{CDOM}(443)$ and $E_{dPAR}(0^+)$) using all of the algorithms tested here, as well as a few combinations of CDM and chlorophyll estimates from different algorithms (see column 4 of Table 1). The lowest RMAD of the estimates was obtained with the GSM outputs. Applying a LUT based on the GSM algorithm or the LUT based on the MBR described above provided visually nearly identical fields of χ_{fluo} (see Fig. 8, described below). We thus kept the simpler approach based on the MBR because of the unexplained results with respect to CDOM when using the GSM and because it did not, except for the iPAR algorithm, rely on the output of a specific algorithm (considering that algorithms may undergo modifications over time).

Fig. 4. Panels are the same as for Fig. 1 but for: A) Φ-corrected OC2M; B) OC3M algorithm; C) Φ-corrected OC3M; D) GSM algorithm; and E) QAA algorithm.

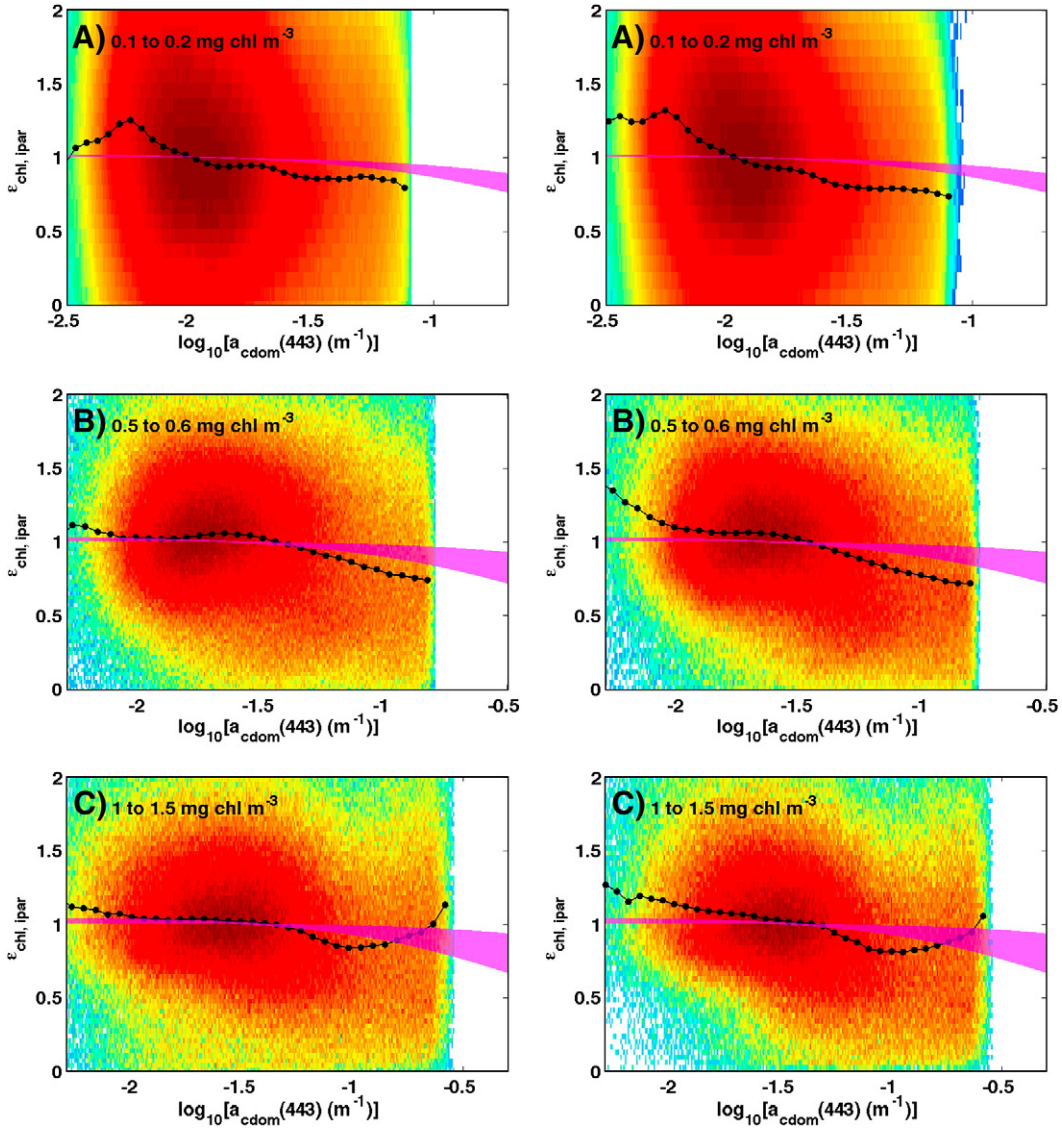

Fig. 5. Panels are the same as for Fig. 3 but for the left panels the chlorophyll was estimated using the Φ-corrected OC2M algorithm to create a surface equivalent to Fig. 2F. For the right panels, the chlorophyll was estimated using the Φ-corrected OC3M to create the surface.

We also examined the possibility of including measures of backscattering (R_{rs}(547), R_{rs}(667), as well as the backscattering coefficient retrieved by the QAA and GSM algorithms) as a fourth dimension in our LUT because high values are known to impact the chlorophyll retrieval (Balch et al., 2005; Brown et al., 2008; Claustre et al., 2002). This was shown to have only a modest impact within restricted regions of high backscattering, for the sake of simplicity we kept a three dimensional LUT because it was a more convenient and computationally efficient solution.

4.4. Applying the algorithm to a global dataset

We applied our χ_{fluo} algorithm using daily Level-3 data for the month of March 2007 and binned the data into a monthly composite (Fig. 8A). Patterns observed often reflect oceanic areas with similar biophysical characteristics of chlorophyll concentration (Fig. 8D), incident irradiance (Fig. 8E), and sea surface temperature (Fig. 8F). Fig. 8B shows the application of a three dimensional LUT-based algorithm to the same dataset but using GSM chlorophyll and CDM estimates as inputs in addition to $E_{dPAR}(0^+)$. Differences between these two panels are very small and would not lead to different interpretations for the vast majority of the ocean. Panel C on the same figure shows the result of applying the NPQ-corrected ϕ_{sat} algorithm of Behrenfeld et al. (2009); this composite was created using Level-3 ocean color data and the color scheme was chosen to match the original publication. The spatial distributions are different for this algorithm compared to our algorithm. Low chlorophyll areas (see Fig. 8D) tend to show higher quantum yields of fluorescence (we did not apply any offset to the data or remove negative values as such differences are expected in the low [*chl*] compared to the original work). This trend is not observed in our approach because, by design, half of the low chlorophyll waters must show lower than average (median) χ_{fluo} and the other half higher than average χ_{fluo}. Outside low chlorophyll areas (which are problematic in any case; we shaded these areas in our maps to reflect this potential problem), differences also appear (see for example the Benguela upwelling and the Southern Ocean). Such differences likely originate from the effect of the $E_{dPAR}(0^+)$, CDOM, and [*chl*] dependencies used. The approach developed in this study attempted to empirically remove these biases. The other source of disparity between the outputs may be inherent to the design of these algorithms. Algorithms based on formulations such as that of Behrenfeld et al. (2009) should in principle (i.e. a theoretically unbiased algorithm) allow the average trend in the quantum yield to be observed as it changes with trophic state. This is not possible with the χ_{fluo} algorithm as this trend is included in the LUT. Therefore, the

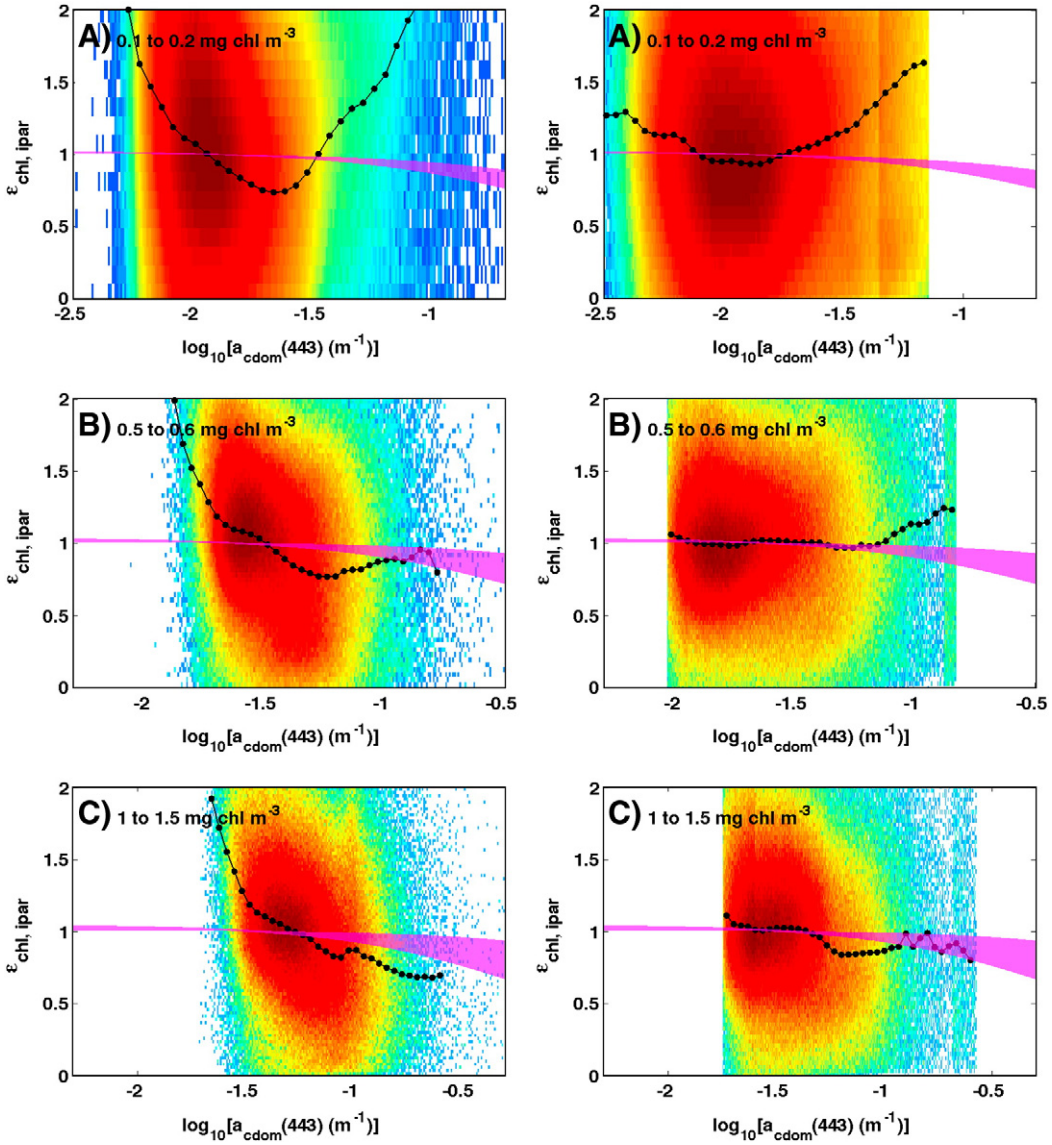

Fig. 6. Panels are the same as for Fig. 3, except that for the left panels the GSM chlorophyll and CDM estimates were used. For the right panels, the QAA chlorophyll and CDM estimates were used. For the latter, the table provided by A. Bricaud (from Bricaud et al., 2004) for the chlorophyll specific absorption coefficient of phytoplankton was used.

present algorithm can only observe differences with respect to the average (median) value for a given trophic state. Whatever the sources of these disparities are, the interpretations of the distributions observed in panels A and C would be different.

4.5. Interpretation of χ_{fluo} (and other quantum yield algorithms)

We can represent the *nFLH* measured by remote sensing as

$$nFLH_{rs}\left(a_{\varphi}, a_{cdm}, E_{dPAR}\right) = \widetilde{nFLH}\left(a_{\varphi,rs}, a_{cdm,rs}, E_{dPAR,rs}\right)\gamma_{nFLH} \quad (5)$$

where $nFLH_{rs}(a_{\varphi},a_{cdm},E_{dPAR})$ is the *nFLH* measured by remote sensing at a given *in situ* a_{φ},a_{CDOM} and E_{dPAR}, $\widetilde{nFLH}\left(a_{\varphi,rs}, a_{cdm,rs}, E_{dPAR,rs}\right)$ is the median *nFLH* in the ocean for the remotely sensed a_{φ}, a_{CDOM} and E_{dPAR} (denoted by the "rs" subscript in the equation) and γ_{nFLH} is a multiplication factor equal to the ratio $nFLH_{rs}\left(a_{\varphi}, a_{cdm}, E_{dPAR}\right)/\widetilde{nFLH}\left(a_{\varphi,rs}, a_{cdm,rs}, E_{dPAR,rs}\right)$. This equation forms the basis of the χ_{fluo} index as comparison with Eq. (4) shows that: $\chi_{fluo}=\gamma_{nFLH}$,$nFLH=nFLH_{rs}(a_{\varphi},a_{cdm},E_{dPAR})$ and $nFLH_{LUT}=\widetilde{nFLH}\left(a_{\varphi,rs}, a_{cdm,rs}, E_{dPAR,rs}\right)$. This representation, however, highlights that γ_{nFLH} (or χ_{fluo}) will incorporate the effect of biases in the remote sensing estimates of a_{φ}, a_{CDOM} and E_{dPAR} relative to the in situ values in addition to variability in the quantum yield that we want to observe (see below).

Using Eq. (1) and assuming that the optical effect of E_{dPAR} is removed by using *nFLH* as a proxy of L_f, we can then use the same logic as above and write:

$$\begin{aligned} nFLH_{rs}\left(a_{\varphi}, a_{cdm}, E_{dPAR}\right) &= cte\cdot a_{\varphi}Q_a^*\varphi_f^{app}\left[\frac{1}{K_{abs}^{\tau_f}+a_f}\right] \\ &= cte\cdot\widetilde{a_{\varphi,rs}}\gamma_a\cdot\widetilde{Q_{a,rs}^*}\gamma_Q\cdot\varphi_{f,rs}^{app}\gamma_{\varphi}\cdot\widetilde{\left[\frac{1}{K_{abs}^{\tau_f}+a_f}\right]_{rs}}\gamma_{K+a} \\ &= \left(cte\cdot\widetilde{a_{\varphi,rs}}\,\widetilde{Q_{a,rs}^*}\,\widetilde{\varphi_{f,rs}^{app}}\widetilde{\left[\frac{1}{K_{abs}^{\tau_f}+a_f}\right]_{rs}}\right)\gamma_a\gamma_Q\gamma_{\varphi}\gamma_{K+a} \end{aligned} \quad (6)$$

where $\widetilde{a_{\varphi,rs}}$, $\widetilde{Q_{a,rs}^*}$, $\widetilde{\varphi_{f,rs}^{app}}$ and $\widetilde{\left[\frac{1}{K_{abs}^{\tau_f}+a_f}\right]_{rs}}$ are the median values of the variables a_{φ},Q_a^*,φ_f^{app} and $\left[\frac{1}{K_{abs}^{\tau_f}+a_f}\right]$ respectively at the median *nFLH* ($nFLH_{LUT}$) for the *MBR*, $^{412}_{443}R_{rs}$ and *iPAR* obtained by remote sensing for a

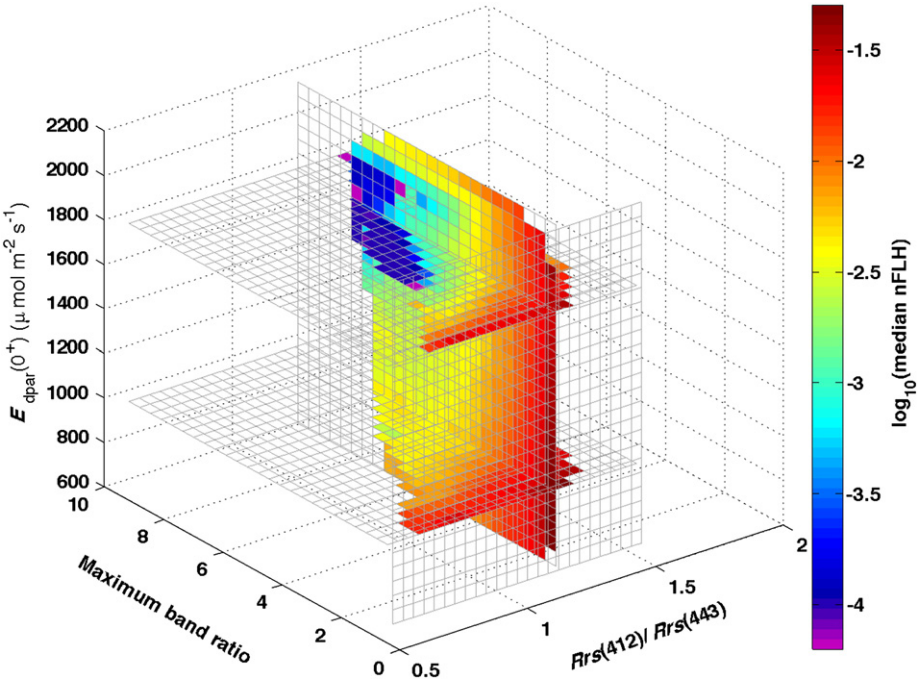

Fig. 7. Slices through the three dimensional lookup table representing the median values of *nFLH* ($nFLH_{LUT}$) with respect to: $E_{dPAR}(0^+)$; the maximum band ratio, which is an index of phytoplankton biomass; and the ratio of $R_{rs}(412)$ to $R_{rs}(443)$, which is an index of CDOM absorption at a given phytoplankton biomass. In the algorithm, for each pixel this lookup table is interpolated to obtain the median value for the remotely measured set of $E_{dPAR}(0^+)$, the maximum band ratio, and $R_{rs}(412)$ to $R_{rs}(443)$. The measured *nFLH* value of a pixel is then divided by the median from the LUT (see Eq. (4)).

given value of in situ a_φ,a_{cdm} and E_{dPAR}; and where $\gamma_a = a_\varphi / \widetilde{a_{\varphi,rs}}$, $\gamma_Q = Q_a^* / \widetilde{Q_{a,rs}^*}$, $\gamma_\varphi = \varphi_f^{app} / \widetilde{\varphi_{f,rs}^{app}}$ and $\gamma_{K+a} = \left[\frac{1}{K_{abs}^{\tau_f} + a_f}\right] \Big/ \widetilde{\left[\frac{1}{K_{abs}^{\tau_f} + a_f}\right]}_{rs}$.

The gammas represent the ratio of the in situ value of a variable to that a median value in the LUT under the remotely estimated proxy of a_φ, a_{CDOM} and E_{dPAR} that are *MBR*, ${}^{412}_{443}R_{rs}$ and E_{dPAR}. By comparison of Eqs. (4), (5) and (6), we see that $\chi_{fluo} = \gamma_{nFLH} = \gamma_a\gamma_Q\gamma_\varphi\gamma_{K+a}$. As such, χ_{fluo} is the product of the ratios of all the variables affecting Sun-induced fluorescence to their median value in the ocean for the same combination of *MBR*, ${}^{412}_{443}R_{rs}$ and *iPAR*. Therefore, χ_{fluo} (and indeed any other estimate of the quantum yield of fluorescence) will represent variability in the quantum yield when γ_a, γ_Q and γ_{K+a} are as close as possible to 1 for all remote sensing conditions. Note that, to simplify this demonstration, we said that ${}^{412}_{443}R_{rs}$ was a measure of a_{cdm}, when in reality it is ${}^{412}_{443}R_{rs}$ at a given MBR that allows an estimate of a_{cdm} (Morel and Gentili, 2009).

5. Discussion

When examining Figs. 1, 2 and 3, one way to evaluate the quality of the retrievals was that the trendlines (median values) followed the theoretical relationship. This theoretical relationship was based on several assumptions. Four of the most uncertain were: 1) that the optical relationships used to describe the mean trend in the ocean were correct, 2) that the apparent quantum yield remained constant with the trophic state, 3) that *nFLH* based on a baseline to extract the fluorescence radiance was not biased with respect to the trophic state of the ocean, and 4) that the *nFLH* could be measured even at the lowest chlorophyll concentration. All of these assumptions could have been incorrect to some degree. In the case of assumptions 1 and 2, it was unlikely that the departures from the assumed constant quantum yield or case 1 water relationships (which were shown to be internally consistent, Morel, 2009) could lead to the shape of the *nFLH* vs chlorophyll relationship at low chlorophyll concentrations observed with OC2M. Similarly, the strong decrease at high chlorophyll observed with some of the algorithms (OC2M, OC3M, and QAA) could not be explained by an incorrect assumption. Quite simply, the case 1 relationships always increase monotonously with chlorophyll and the changes in the quantum yield would have to be unrealistically large and systematic to account for such departures. This assessment was supported by the observation that correcting the empirical algorithm for the effect of CDM reduced the biases. Assumptions 3 and 4 were much harder to dismiss as theoretical calculations have shown that at low chlorophyll concentrations: a) there is a bias of ~50% in the estimate of the fluorescence line height (Huot et al., 2005), which would induce an underestimate of the radiance observed (and not an overestimate as was the case for the flooring observed with the empirical algorithms); and b) we were reaching the prelaunch requirement for the noise equivalent radiance of the MODIS sensor and the measurement might have simply been meaningless (Babin et al., 1996; Letelier and Abbott, 1996). Point *a* cannot be assessed with the present analyses. We attempted to address point b in Appendix 2 and found that with the 4 km resolution Level-3 data used in the present study, the limit of detection should be around 0.04 to 0.15 mg chl m^{-3}. We thus suggest that data from regions with chlorophyll concentrations below approximately 0.1 mg chl m^{-3} be considered tentative. When averages are computed for a large number of points, meaningful values may still, however, be obtained below this limit, such as in Figs. 1 and 3.

Analyses such as the one presented in Table 1 highlight the potential of using fluorescence emission to tune ocean color algorithms to retrieve chlorophyll or phytoplankton absorption. Everything else being equal, an estimate of chlorophyll or phytoplankton absorption that explains more of the variability in the *nFLH* should be considered a better algorithm to retrieve phytoplankton biomass. A similar suggestion was also previously made by Behrenfeld et al. (2009). In this approach, there is no need to assume any functional relationship between phytoplankton absorption or biomass and fluorescence emission.

The χ_{fluo} algorithm we have presented here to retrieve the variability in the quantum yield of fluorescence was very different, and in

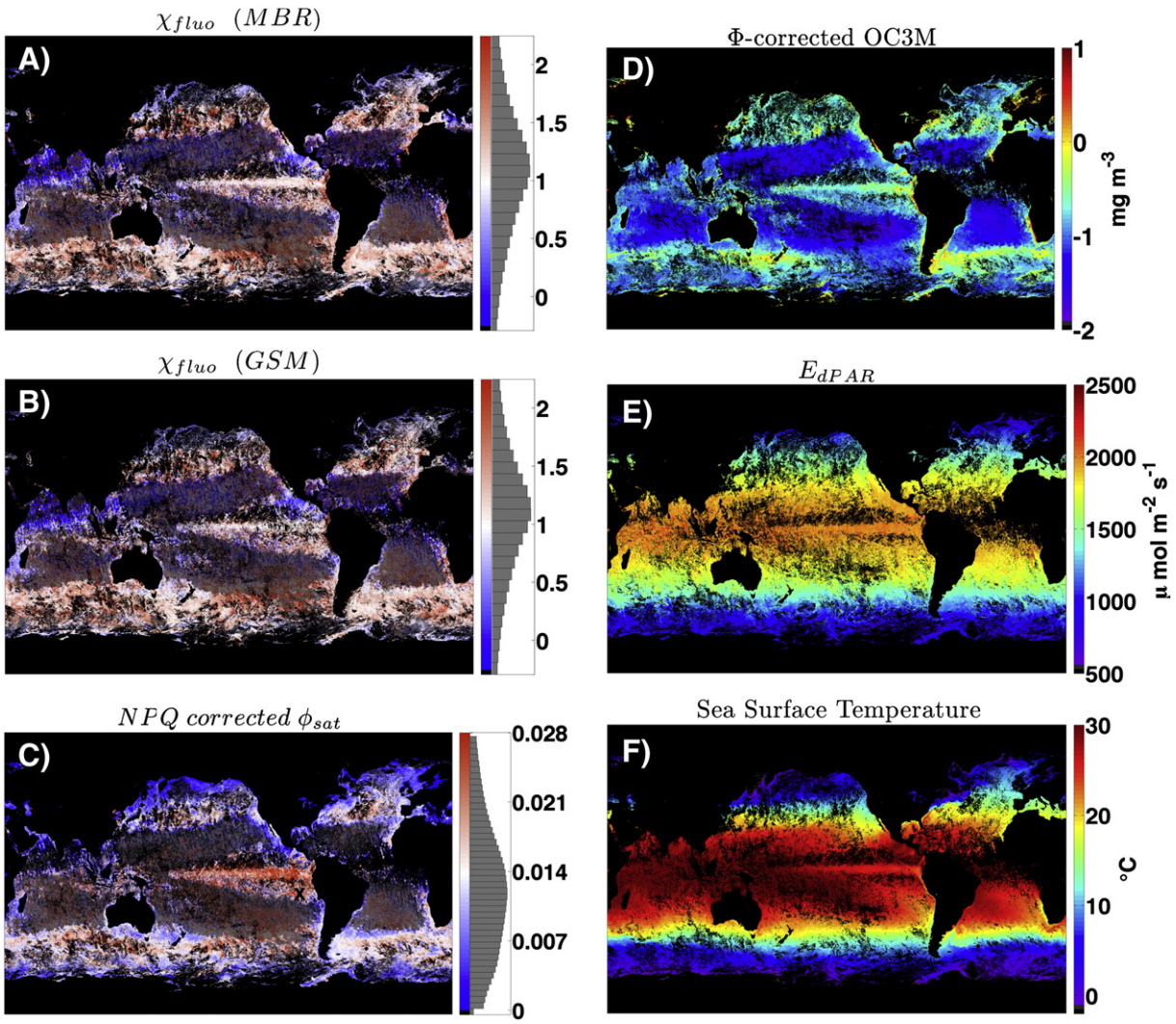

Fig. 8. Global distributions for the month of March 2007 of: A) variation in χ_{fluo} (see Eq. (4)); B) variation in χ_{fluo} when the GSM outputs were used for chlorophyll and CDM were used (instead of the MBR and the ratio of R_{rs} at 412 and 443 nm); C) quantum yield of fluorescence computed using the algorithm presented by Behrenfeld et al. (2009, their Eq. (A12)); D) Φ-corrected OC3M chlorophyll estimates; F) $E_{dPAR}(0^+)$ from the iPAR algorithm; and G) sea surface temperatures.

many ways superior, to that proposed by Huot et al. (2005), which inspired subsequent variations (Behrenfeld et al., 2009; Morrison and Goodwin, 2010). In the present study, our algorithm was based directly on observations and did not make any assumptions about the average global optical characteristics of the water as a function of remotely sensed chlorophyll or potential biases in the measurement of L_f (see Eq. (1)) by *nFLH* because they were all inherently accounted for. Furthermore, we corrected as much as possible for the effects of CDM on *nFLH* by using what we believed was one of the most accurate methods based on our study. The algorithm was also more robust with respect to calibration errors (as long as they remains stable) of the sensor or possible biases in the algorithms and proxies for [*chl*], $a_{CDOM}(443)$, and $E_{dPAR}(0^+)$ because the LUT inherently accounted for many of these biases. As long as the proxy was functionally related to the "true" value, the LUT should have been able to account for the biases. As an example, if an algorithm for [*chl*] retrieves on average values that are two times too high over a certain range of [*chl*] this would lead to quantum yields that are two times too low in that range of [*chl*] using previous quantum yield algorithms. Such biases are not present in the LUT approach developed here. This property, stemming from the design of the algorithm, is also interesting from the perspective of merging data from multiple sensors. Indeed, as long as a satellite can provide robust proxies of [*chl*], $a_{CDOM}(443)$, and $E_{dPAR}(0^+)$ that are functionally related to those of MODIS, the resulting fields of χ_{fluo} should be sufficiently similar for merging the data. This was at least partially confirmed by comparing the LUTs based on the MBR and GSM outputs (Fig. 8A and B). This said, we do not believe that the algorithm presented by Huot et al. (2005) and subsequent improvements are fundamentally flawed from a theoretical point of view; however, we think that the details of the implementations (including the relationships for case 1 waters, the ocean color algorithms used to retrieve [*chl*] or a_{φ}, and potential measurement biases) may lead to biases.

The apparent downside of the LUT-based algorithm was that it did not provide quantum yields in absolute values. Although this is somewhat unfortunate because Sun-induced fluorescence theory allows its calculation, comparison of the absolute quantum yield with other measurements of the absolute quantum yield, apart from those taken with radiometers in situ, has not been carried out to this day. Indeed, absolute quantum yield measurements are almost never carried out in the laboratory (though proxies have been obtained e.g. Cleveland and Perry, 1987; Laney et al., 2005). Standard methods to measure variable fluorescence in the lab, such as pulse amplitude modulation (PAM) fluorometry or fast repetition rate (FRR) fluorometry, are not generally interpreted in terms of absolute quantum yields (especially not apparent quantum yields such as is the case when Sun-induced quantum yields

are measured Huot and Babin, 2010). In fact, not capturing the variability caused by the mean trend with trophic level could turn out to be an advantage as regions with different trophic regimes can be compared more easily. Current interpretations (e.g. Behrenfeld et al., 2009; Morrison and Goodwin, 2010) of the quantum yields are more consistent with the χ_{fluo} product than with the results of an algorithm that could show changes with trophic levels.

Several other limitations must be kept in mind when using this algorithm. Because the algorithm corrects as much as possible for the effect of $E_{dPAR}(0^+)$ at the time of the overpass, and therefore indirectly for the mean PAR irradiance received during the day, it is not possible to study photocompensation mechanisms (e.g. Morrison and Goodwin, 2010) without taking special care. Indeed, such an analysis could be carried out, for example by fixing the PAR value to a constant and studying the resulting variability in χ_{fluo}. The limits of estimates of *nFLH* for case 2 waters have been well documented (Gilerson et al., 2008; Ioannou et al., 2009) and we will not discuss them here, except to say that the low quantum yields often observed near the coast and in estuaries in Fig. 8 are likely the result of uncorrected biases in these waters.

We worked with daily Level-3 data to develop our LUT and thus our algorithm can be readily applied to obtain global distributions of χ_{fluo} from existing products distributed by NASA without significant computational effort. The primary disadvantage of working with Level-3 products is that fluorescence specific bidirectional effects (Morel et al., 2002; Park and Ruddick, 2005) could not be corrected. This could be a significant source of variability since the bidirectional correction currently applied to the measured water leaving radiance only corrects for elastic scattering and Raman scattering (using tables from Morel et al., 2002) and this does not correct appropriately the fluorescence emission. Including the viewing angle in the LUT (which would be applied during the Level-2 processing) could, thus, further reduce the scatter. Another disadvantage was that we had to work with the fluorescence proxy that was available, namely *nFLH*. Using a measure of fluorescence based on radiances, instead of normalized water leaving radiances, may also help to slightly reduce scatter in the data. Lastly, working with Level-3 products as distributed, we had to use above water incident irradiance ($E_{dPAR}(0^+)$) as we cannot account for the Sun zenith angle to compute the transmission at the air–sea interface. Since the main driver of the underwater irradiance is $E_{dPAR}(0^+)$ and the air–sea transmission is largely affected (through the zenith angle of the Sun) by $E_{dPAR}(0^+)$ the effect of not accounting for the transmission through the interface is likely small on the retrieved χ_{fluo}. Nevertheless, in the future, the use of $E_{dPAR}(0^-)$ would provide some reduction of the scatter. In any case, it is very unlikely that these potential future improvements will lead to a large change in the patterns observed but would most likely slightly reduce the scatter in the resulting χ_{fluo}. The LUT approach developed in this study allows the inclusion of other variables and only requires recomputing the LUT, which could easily be done in an operational setting.

6. Conclusions

Despite the availability of spaceborne Sun-induced fluorescence data for more than a decade, very little insight into the functioning of the ocean has been gained from these observations. The disinclination of the ocean color community to use algorithms estimating the quantum yield of fluorescence is likely due to the possibility of biases in these data. Despite these hurdles, two interesting contributions by Behrenfeld et al. (2009) and Morrison and Goodwin (2010) have identified iron limitation and "photocompensation" mechanisms respectively as potential causes of variability in the signal that could be exploited to study aspects of phytoplankton ecophysiology from space. These studies have highlighted that identifying the biological sources of variability in the quantum yield could indeed lead to a very powerful tool to study the oceans from space. While more validation is required to use Sun-induced fluorescence as a diagnostic tool, the algorithm presented in this study eliminates some of the biases that were present in previous algorithms. On theoretical grounds, it is an improvement over previous algorithms in the following regards:

1) it does not assume case 1 water relationships (as good as they may be);
2) it accounts for the effect of variability in the CDM absorption on a pixel-by-pixel basis as it affects, on average, the emission of fluorescence;
3) it provides a more accurate representation of the mean effect of incident irradiance on *nFLH;*
4) it accounts for any biases that may arise at low chlorophyll concentration;
5) it accounts fully for the cross terms of phytoplankton absorption, incident PAR irradiance, and CDM;

As such, it should provide more reliable estimates of variability in the quantum yield, which is critical to interpreting its distribution spatially, as well as its variability temporally.

Appendix 1. Calculating the impact of CDOM on Sun-induced fluorescence emission

The fluorescence radiance just beneath the surface of the ocean is given by Eq. (1). The impact of CDOM on most oceanic waters is through its effect on the absorption of light at the surface and thus the reduced or increased availability of light to phytoplankton and consequently, fluorescence. This effect is expressed by the term $K_{abs}^{\tau_f}$ which represents the attenuation of the light absorbed by phytoplankton over the region where 90% of the fluorescence radiance originates. The attenuation of upwelling radiance in the fluorescence band represented by the term a_f is, in principle, also affected by CDOM; however, in most oceanic water this effect is negligible due to the low absorption by CDOM near 683 nm relative to the absorption by water.

At a given chlorophyll concentration or phytoplankton absorption the ocean contains an average CDOM (Morel, 2009; Morel and Gentili, 2009) and CDM (Siegel et al., 2005) concentration. If we assume that the quantum yield to remains constant and we take the ratio (γ_{CDOM}) of the fluorescence radiance (Eq. (1)) emitted with a given concentration of CDOM (variables with a superscript $\Delta CDOM$) to the fluorescence emitted with an average concentration (variables with an overbar), we obtain Eq. (3). To model the average trends, the average absorption of CDOM and detrital material at 400 nm as a function of chlorophyll concentration has been obtained from Morel (2009) as

$$\overline{a}_y(400,[chl]) = 0.065[chl]^{0.63} \quad \text{A1}$$

which can be extended spectrally by using an exponentially decreasing function as

$$\overline{a}_y(\lambda,[chl]) = 0.065[chl]^{0.63}\cdot e^{(-S(\lambda-400))}. \quad \text{A2}$$

where S is the exponential slope of the CDOM absorption, taken as 0.018 nm^{-1} here.

Using this information, we can modify the mean spectral downwelling diffuse attenuation (K_d, m^{-1}) coefficient given by Morel and Maritorena (2001). To do so we use the coefficients for K_{bio} from (Morel et al., 2007) as follows $K_d = K_w + K_{bio} + f_{CDOM}\cdot a_y/\mu_d$ where K_w is the diffuse attenuation coefficient for water and K_{bio} the diffuse attenuation coefficient for chlorophyll and covarying matter, and f_{CDOM} is a coefficient equal to ${}^{\Delta CDOM}a_y/\overline{a}_y - 1$, where ${}^{\Delta CDOM}a_y$ is the absorption of CDOM when CDOM is not equal to the mean oceanic value ($\overline{a}_y$) for that chlorophyll concentration, hence $f_{CDOM} = 0$ represents the average value. Note that the term K_{bio}, already accounts for the mean oceanic concentration at a given chlorophyll concentration as such f_{CDOM} represents a fractional

increase or decrease relative to the mean. Finally, the $\overline{a}_y/\mu_d$ represents the partial diffuse attenuation coefficient from the mean concentration of CDOM in the ocean at a given chlorophyll concentration.

Using these relationships, we computed the spectral attenuation coefficient as affected by CDOM absorption for 0.15, 0.55 and 1.25 mg chl m^{-3}. Based on this diffuse attenuation coefficient and the spectral absorption coefficient of phytoplankton provided by Bricaud et al. (1995 with updated coefficients in 2004) we computed the attenuation of spectral irradiance absorbed by phytoplankton with depth. We then proceeded with the iterative computation described in Huot et al. (2005) to compute $K_{abs}^{T_f}$.

Using these $K_{abs}^{T_f}$ values as well as the appropriate a_f for each chlorophyll concentration, we computed γ_{CDOM}. To provide estimates of the maximum and minimum values for γ_{CDOM} we recomputed a_y using Eq. (A1) by changing the chlorophyll dependency from 0.63 to 0.56 and 0.7 and the value of a_y at 1 m chl m^{-3} and 400 nm from 0.065 m^{-1} to 0.078 and 0.052 m^{-1}. Using these simulations, a region representing the effect of CDOM was defined as the maximum and minimum values of Eq. (3) for each CDOM absorption value and is represented in Fig. 3 (and other similar figures) by the magenta area.

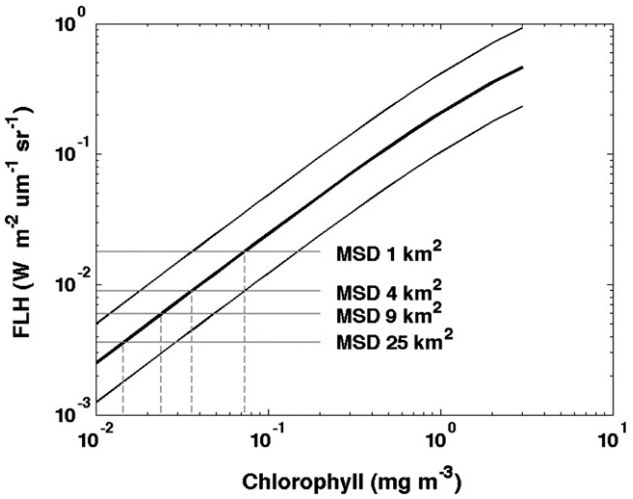

Fig. A1. Relationship between FLH and chlorophyll concentration (thick black line). Horizontal lines represents the calculated minimum signal of detection of the FLH for 1, 4, 9 and 25 pixels (1 km^2, 4 km^2, 9 km^2 and 25 km^2), the vertical dashed line represents an estimate of the chlorophyll concentration at which this FLH would be obtained. The thin black lines parallel to the thick black line represent a factor of two greater (upper line) and lower (lower line) quantum yield of fluorescence.

Appendix 2. Limit of detection for MODIS

The limit of detection on the MODIS instrument in terms of fluorescence line height (FLH) at 676.7 nm (Letelier and Abbott, 1996) and radiance at 682 nm (Babin et al., 1996) was been evaluated before its launch. Working with the data available at the time regarding the expected sensor characteristics (required signal to noise ratio), top of atmosphere (TOA) radiance and quantum yield of fluorescence in surface waters, these studies suggested that MODIS would be able to detect the top of the atmosphere FLH down to about 0.012 W m^{-2} sr^{-1} μm^{-1} (Letelier and Abbott, 1996) and the upwelling radiance at 682 nm down to about 0.008 W m^{-2} sr^{-1} μm^{-1} (Babin et al., 1996). These values, once propagated below the water surface and compared with estimated emission by phytoplankton returned detection limits of Sun-induced fluorescence from waters with chlorophyll concentrations of ~0.5 mg chl m^{-3} (Letelier and Abbott, 1996) and 0.07 mg chl m^{-3} (Babin et al., 1996).

Recomputing the TOA detection limit using the actual MODIS characteristics (cf. Franz et al., 2006) and a computation identical to that used by Letelier and Abbott (1996), leads to a detection limit for FLH at the TOA of 0.014 W m^{-2} sr^{-1} μm^{-1}. Despite the slightly higher signal to noise values used here, the result is slightly above that computed by Letelier and Abbott (1996), because the typical TOA radiance used is higher. To find the correspondance between this TOA fluorescence radiance and biomass in terms of chlorophyll is more difficult. For this calculation, we assume that the TOA fluorescence radiance is equal to the previously distributed FLH product used in Huot et al. (2005), that is, TOA radiance corrected for Rayleigh scattering losses. We use, as a benchmark, the simple relationship derived by Gower et al. (their Eq. (4)), which, once multiplied by 1.65, was shown to match very well the relationship between chlorophyll and FLH for the region west of Central America (2005). Using this relationship, we find a chlorophyll concentration of 0.073 mg chl m^{-3} as the limit of detection (see Fig. A1). A factor of at least 2 is clearly possible in this estimate depending on the region (Huot et al., 2005, compare their Fig. 13 vs Fig. 9) and dispersion within a region (upper and lower thin lines in Fig. A1). Therefore, we could say that the limit of detection is anywhere between 0.035 and 0.14 mg chl m^{-3}. However, it is impossible to know, for a given pixel, what this limit is based solely on the chlorophyll estimate (it depends, amongst other things, on the physiology of the phytoplankton observed). Therefore, as a first semi-quantitative delineation, we should consider any data below ~0.15 mg chl m^{-3} as suspicious at 1 km resolution.

A different approach to assess the limit of detection is studying the variability in *nFLH* as a function of the *nFLH* itself. In order to do this, we computed the standard deviation (std($nFLH_{25}$)) and the mean (mean($nFLH_{25}$)) of 273,383 groups of 25 adjacent pixels taken from 16 level 2 dataset (distributed on the ocean color website) selected to represent different regions and trophic state of the ocean. We plotted the mean over the standard deviation of this dataset as a function of chlorophyll and *nFLH* (Fig. A2). The variability seen in these figures is originates from the spatial variability in the fluorescence signal (including that caused by the algorithm) and the sensor noise. At high *nFLH* values, the sensor noise should be negligible and the variability minimum as is observed in Fig. A2 (mean/standard deviation ~ 10). As the *nFLH* decreases, the influence of sensor noise increases, and this is reflected in a rapid decrease in the signal to noise ratio (Fig. A2). If we

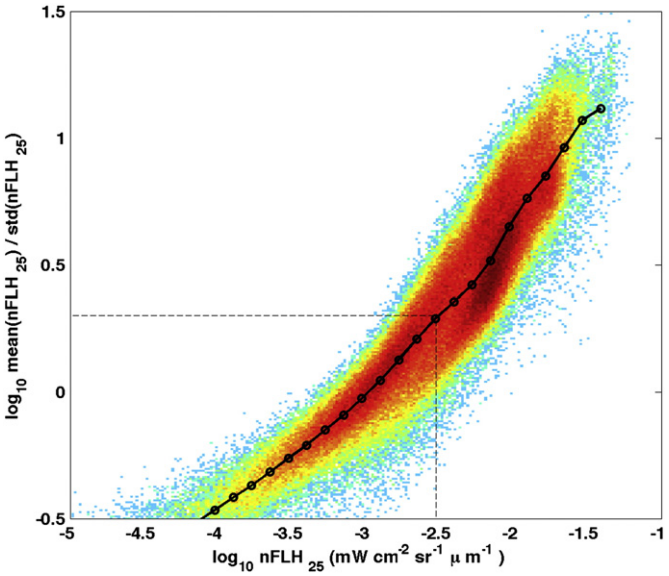

Fig. A2. Density plot of the ratio of the mean to the standard deviation of groups of 25 adjacent pixels (a measure of the signal to noise in the data) as a function of the mean of the groups. The continuous line with dots is a line representing the median trendline (see Fig. 1 and accompanying text). The vertical dashed line is the *nFLH* value (0.003 mW cm^{-2} sr^{-1} μm^{-1}) at which 50% of the points have a mean to standard deviation ratio of 2 (horizontal dashed line).

consider, for example, that a ratio of the signal to noise greater than 2 is required for at least 50% of the points, we find that the minimum *nFLH* is around 0.003 mW cm^{-2} sr^{-1} μm^{-1} (which corresponds very roughly to 0.1 mg chl m^{-3}, see Fig. 1). Such a limit, in terms of *nFLH* and based on the measured *nFLH* value provides a more accurate way of separating points that are above the detection limit. A similar analysis in terms of FLH would probably provide an even more reliable estimate of the lower limit of detection (i.e. not influenced by the incident irradiance), however, since *nFLH* are presently distributed by NASA, we carried out the analysis on *nFLH* data.

References

Abbott, M. R., & Letelier, R. M. (1999). *Algorithm theoretical basis document chlorophyll fluorescence (MODIS product number 20)*. NASA.

Ahmad, Z., McClain, C. R., Herman, J. R., Franz, B. A., Kwiatkowska, E. J., Robinson, W. D., et al. (2007). Atmospheric correction for NO_2 absorption in retrieving water-leaving reflectances from the seawifs and MODIS measurements. *Applied Optics*, *46*(26), 6504–6512.

Ahn, Y. H., & Shanmugam, P. (2007). Derivation and analysis of the fluorescence algorithms to estimate phytoplankton pigment concentrations in optically complex coastal waters. *Journal of Optics A: Pure and Applied Optics*, *9*, 352–362.

Antoine, D., Morel, A., Gordon, H. R., Banzon, V. F., & Evans, R. H. (2005). Bridging ocean color observations of the 1980s and 2000s in search of long-term trends. *Journal of Geophysical Research-Oceans*, *110*, C06009. http://dx.doi.org/10.1029/2004JC002620.

Babin, M., Morel, A., & Gentili, B. (1996). Remote sensing of sea surface sun-induced chlorophyll fluorescence: Consequences of natural variations in the optical characteristics of phytoplankton and the quantum yield of chlorophyll a fluorescence. *International Journal of Remote Sensing*, *17*(12), 2417–2448.

Balch, W. M., Gordon, H. R., Bowler, B. C., Drapeau, D. T., & Booth, E. S. (2005). Calcium carbonate measurements in the surface global ocean based on moderate-resolution imaging spectroradiometer data. *Journal of Geophysical Research-Oceans*, *110*, C07001.

Behrenfeld, M. J., Westberry, T. K., Boss, E. S., O'Malley, R. T., Siegel, D. A., Wiggert, J. D., et al. (2009). Satellite-detected fluorescence reveals global physiology of ocean phytoplankton. *Biogeosciences*, *6*, 779–794.

Bricaud, A., Babin, M., Morel, A., & Claustre, H. (1995). Variability in the chlorophyll-specific absorption coefficients of natural phytoplankton: Analysis and parameterization. *Journal of Geophysical Research-Oceans*, *100*(C7), 13321–13332.

Bricaud, A., Claustre, H., Ras, J., & Oubelkheir, K. (2004). Natural variability of phytoplankton absorption in oceanic waters: Influence of the size structure of algal populations. *Journal of Geophysical Research-Oceans*, *109*, C11010. http://dx.doi.org/10.1029/2004JC002419.

Brown, C. A., Huot, Y., Werdell, J. P., Gentili, B., & Claustre, H. (2008). The origin and global distribution of second order variability in satellite ocean color and its potential applications to algorithm development. *Remote Sensing of Environment*. http://dx.doi.org/10.1016/j.rse.2008.06.008.

Carder, K. L., Chen, F. R., & Hawes, S. K. (2003). *Algorithm theoretical basis document ATBD 20 instantaneous photosynthetically available radiation and absorbed radiation by phytoplankton*. NASA.

Carder, K. L., Hawes, S. K., Baker, K. A., & Smith, R. (1991). *Reflectance model for quantifying chlorophyll a in the presence oi productivity degradation products*.

Clarke, G. L., Ewing, G. C., & Lorenzen, C. J. (1970). Spectra of backscattered light from the sea obtained from aircraft as a measure of chlorophyll concentration. *Science (New York, N.Y.)*, *167*(3921), 1119–1121.

Claustre, H., Morel, A., Hooker, S. B., Babin, M., Antoine, D., Oubelkheir, K., et al. (2002). Is desert dust making oligotrophic waters greener? *Geophysical Research Letters*, *29*(10), 107-1. http://dx.doi.org/10.1029/2001GL014056.

Cleveland, J. S., & Perry, M. J. (1987). Quantum yield, relative specific absorption and fluorescence in nitrogen-limited chaetoceros gracilis. *Marine Biology*, *94*, 489–497.

Franz, B. A., Werdell, P. J., Meister, G., Kwiatkowska, E. J., Bailey, S. W., Ahmad, Z., et al. (2006). MODIS land bands for ocean remote sensing applications. *Proc. Ocean optics XVIII, Vol. 10*, Canada: Montreal.

Garver, S. A., & Siegel, D. A. (1997). Inherent optical property inversion of ocean color spectra and its biogeochemical interpretation 1. Time series from the sargasso sea. *Journal of Geophysical Research*, *102*(C8), 18607–18625.

Gilerson, A., Zhou, J., Hlaing, S., Ioannou, I., Gross, B., Moshary, F., et al. (2008). Fluorescence component in the reflectance spectra from coastal waters. II. Performance of retrieval algorithms. *Optics Express*, *16*(4), 2446–2460.

Gilerson, A., Zhou, J., Hlaing, S., Ioannou, I., Schalles, J., Gross, B., et al. (2007). Fluorescence component in the reflectance spectra from coastal waters. Dependence on water composition. *Optics Express*, *15*(24), 15702–15721.

Gordon, H. R. (1989). Can the Lambert–Beer law be applied to the diffuse attenuation coefficient of ocean water? *Limnology and Oceanography*, *34*(8), 1389–1409.

Gordon, H. R., Brown, O. B., Evans, R. H., Brown, J. W., Smith, R. C., Baker, K. S., et al. (1988). A semianalytic radiance model of ocean color. *Journal of Geophysical Research-Oceans*, *93*(D9), 10909–10924.

Gordon, H. R., & Wang, M. (1994). Retrieval of water-leaving radiance and aerosol optical thickness over the oceans with seawifs: A preliminary algorithm. *Applied Optics*, *33*(3), 443–452.

Gower, J. F. R., & Borstad, G. A. (2004). On the potential of MODIS and MERIS for imaging chlorophyll fluorescence from space. *International Journal of Remote Sensing*, *25*(7), 1459–1464.

Gower, J. F. R., Brown, L., & Borstad, G. A. (2004). Observations of chlorophyll fluorescence in west coast waters of canada using the MODIS satellite sensor. *Canadian Journal of Remote Sensing*, *30*(1), 17–25.

Huot, Y., & Babin, M. (2010). Overview of fluorescence protocols: Theory, basic concepts, and practice. *Chlorophyll a fluorescence in aquatic sciences: Methods and applications* (pp. 31–74). Dordrecht: Springer Netherlands. http://dx.doi.org/10.1007/978-90-481-9268-7_3.

Huot, Y., Brown, C. A., & Cullen, J. J. (2005). New algorithms for MODIS sun-induced chlorophyll fluorescence and a comparison with present data products. *Limnology and Oceanography: Methods*, *3*, 108–130.

Huot, Y., Brown, C. A., & Cullen, J. J. (2007). Retrieval of phytoplankton biomass from simultaneous inversion of reflectance, the diffuse attenuation coefficient, and sun-induced fluorescence in coastal waters. *Journal of Geophysical Research-Oceans*, *112*(C6).

Ioannou, I., Zhou, J., Gilerson, A., Gross, B., Moshary, F., & Ahmed, S. (2009). New algorithm for MODIS chlorophyll fluorescence height retrieval: Performance and comparison with the current product (proceedings paper). *Proceedings of SPIE: Remote sensing of the ocean, sea ice, and large water regions*, *vol. 7473*, SPIE. http://dx.doi.org/10.1117/12.830630.

IOCCG (2006). Remote sensing of inherent optical properties: Fundamentals, tests of algorithms, and applications. Dartmouth, Canada: IOCCG.

Kishino, M., Sugihara, S., & Okami, N. (1984). Influence of fluorescence of chlorophyll a on underwater upward irradiance spectrum. *La Mer*, *22*, 224–232.

Krause, G. H., & Jahns, P. (2004). Non-photochemical energy dissipation determined by chlorophyll fluorescence quenching: Characterization and function. In G. C. Papageorgiou, & G. Govindjee (Eds.), *Chlorophyll a fluorescence: A signature of photosynthesis* (pp. 463–495). Springer.

Laney, S. R., Letelier, R. M., & Abbott, M. R. (2005). Parameterizing the natural fluorescence kinetics of *Thalassiosira weissflogii*. *Limnology and Oceanography*, *50*, 1499–1510.

Lee, Z. P., Carder, K. L., & Arnone, R. A. (2002). Deriving inherent optical properties from water color: A multiband quasi-analytical algorithm for optically deep waters. *Applied Optics*, *41*(27), 5755–5772.

Lee, Z. -P., & Hu, C. (2006). Global distribution of case-1 waters: Analysis from seawifs measurements. *Remote Sensing of Environment*, *101*, 270–276.

Letelier, R., & Abbott, M. R. (1996). An analysis of chlorophyll fluorescence algorithms for the moderate resolution imaging spectrometer (MODIS). *Remote Sensing of Environment*, *58*, 215–223.

Letelier, R. M., Abbott, M. R., & Karl, D. M. (1997). Chlorophyll fluorescence response to upwelling events in the southern ocean. *Journal of Geophysical Research*, *24*(4), 409–412.

Maritorena, S., Morel, A., & Gentili, B. (2000). Determination of the fluorescence quantum yield by oceanic phytoplankton in their natural habitat. *Applied Optics*, *39*(36), 6725–6737.

Maritorena, S., Siegel, D. A., & Peterson, A. R. (2002). Optimization of a semianalytical ocean color model for global-scale applications. *Applied Optics*, *41*(15), 2705–2714.

McKee, D., Cunningham, A., Wright, D., & Hay, L. (2007). Potential impacts of nonalgal materials on water-leaving sun induced chlorophyll fluorescence signals in coastal waters. *Applied Optics*, *46*(31), 7720–7729.

Morel, A. (1980). In-water and remote measurements of ocean color. *Boundary-Layer Meteorology*, *18*(2), 177–201.

Morel, A. (1988). Optical modeling of the upper ocean in relation to its biogenous matter content (case 1 waters). *Journal of Geophysical Research-Oceans*, *93*(C9), 10749–10768.

Morel, A. (2009). Are the empirical relationships describing the bio-optical properties of case 1 waters consistent and internally compatible. *Journal of Geophysical Research — Oceans*, 114.

Morel, A., Antoine, D., & Gentili, B. (2002). Bidirectional reflectance of oceanic waters: Accounting for raman emission and varying particle scattering phase function. *Applied Optics*, *41*(30), 6289–6306.

Morel, A., & Gentili, B. (2009). A simple band ratio technique to quantify the colored dissolved and detrital organic material from ocean color remotely sensed data. *Remote Sensing of Environment*, *113*(5), 998–1011.

Morel, A. Y., & Gordon, H. R. (1980). Report of the working group on water color. *Boundary Layer Meteorology*, 18.

Morel, A., Huot, Y., Gentili, B., Werdell, P. J., Hooker, S. B., & Franz, B. A. (2007). Examining the consistency of products derived from various ocean color sensors in open ocean (case 1) waters in the perspective of a multi-sensor approach. *Remote Sensing of Environment*, *111*(1), 69–88.

Morel, A., & Maritorena, S. (2001). Bio-optical properties of oceanic waters: A reappraisal. *Journal of Geophysical Research-Oceans*, *106*(C4), 7163–7180.

Morel, A., & Prieur, L. (1977). Analysis of variations in ocean color. *Limnology and Oceanography*, *22*, 709–722.

Morrison, J. R. (2003). In situ determination of the quantum yield of phytoplankton chlorophyll a fluorescence: A simple algorithm, observations, and a model. *Limnology and Oceanography*, *48*(2), 618–631.

Morrison, J. R., & Goodwin, D. S. (2010). Phytoplankton photocompensation from space-based fluorescence measurements. *Geophysical Research Letters*, *37*(6), L06603.

O'Reilly, J. E., Maritorena, S., Mitchell, B. G., Siegel, D. A., Carder, K. L., Garver, S. A., et al. (1998). Ocean color chlorophyll algorithms for seawifs. *Journal of Geophysical Research-Oceans*, *103*(C11), 24937–24953.

Ostrowska, M., Darecki, M., & Wozniak, B. (1997). An attempt to use measurements of sun-induced chlorophyll fluorescence to estimate chlorophyll a concentration in the baltic sea. *Proceedings of SPIE The International Society for Optical Engineering*, *3222*, 528–537.

Park, Y., & Ruddick, K. (2005). Model of remote-sensing reflectance including bidirectional effects for case 1 and case 2 waters peer reviewed article. *Applied Optics*, *44*(7), 1236–1249.

Roesler, C. S., & Perry, M. J. (1995). In situ phytoplankton absorption, fluorescence emission, and particulate backscattering spectra determined from reflectance. *Journal of Geophysical Research-Oceans*, *100*(C7).

Rousseeuw, P. J., & Croux, C. (1993). Alternatives to the median absolute deviation. *Journal of the American Statistical Association*, *88*(424), 1273–1283.

Sathyendranath, S., Platt, T., Irwin, B., Horne, E., Borstad, G. A., Stuart, V., et al. (2004). A multispectral remote sensing study of coastal waters off vancouver island. *International Journal of Remote Sensing*, *25*(5), 893–919.

Schallenberg, C., Lewis, M. R., Kelley, D. E., & Cullen, J. J. (2008). The inferred influence of nutrient availability on the relationship between sun-induced fluorescence and incident irradiance in the bering sea. *Journal of Geophysical Research*, *113*, C07046.

Siegel, D. A., Maritorena, S., Nelson, N. B., Behrenfeld, M. J., & McClain, C. R. (2005). Colored dissolved organic matter and its influence on the satellite-based characterization of the ocean biosphere. *Geophysical Research Letters*, *32*(20), L20605.

Siegel, D. A., Maritorena, S., Nelson, N. B., Hansell, D. A., & Lorenzi-Kayser, M. (2002). Global distribution and dynamics of colored dissolved and detrital organic materials. *Journal of Geophysical Research*, *107*(C12), 3228.

Thuillier, G., Herse, M., Labs, D., Foujols, T., Peetermans, W., Gillotay, D., et al. (2003). The solar spectral irradiance from 200 to 2400 nm as measured by the solspec spectrometer from the ATLAS and EURECA missions. *Solar Physics*, *214*, 1–22.

Yentsch, C. S. (1960). The influence of phytoplankton pigments on the colour of sea water. *Deep Sea Research*, *7*, 1–9.

Zhou, J., Gilerson, A., Ioannou, I., Hlaing, S., Schalles, J., Gross, B., et al. (2008). Retrieving quantum yield of sun-induced chlorophyll fluorescence near surface from hyperspectral in-situ measurement in productive water. *Optics Express*, *16*(22), 17468–17483.